Tampere University

Tran Nguyen Le

Force Control for Soft Robotic Hands Applied to Grasping

Abstract

Tran Nguyen Le: Force Control for Soft Robotic Hands Applied to Grasping
Master's thesis
Tampere University
Master of Science (Technology) - Factory Automation and Industrial Informatics
August 2019

Robotic grasping has been studied for more than 30 years, but it is still a challenging field. Today, most robotic grippers are rigid, making it hard for them to grasp and handle irregularly shaped objects that are delicate and easily deformed such as a compact disc, an egg, or an empty plastic cup. To tackle this issue, soft robotic hands have been introduced. Despite advantages of soft robotic hands, their applications are still limited to simple pick-and-place tasks. The main reason for this is their lack of sensing capabilities, which leads to the absence of information about the internal state of the hand or the interaction between the hand and the environment. This thesis aims to tackle this issue by integrating appropriate sensors into a soft robotic hand. The information extracted from the sensory readings is then used to develop a control strategy to study the interaction between the hand and objects. Experiments performed on the developed soft hand and controller board showed that the interaction between the hand and objects could be studied by using only sensors integrated into the hand. The final results also showed that this information could be used to successfully control the soft hand in real time to achieve a manipulation task such as grasping deformable planar objects especially thin-shell objects like empty plastic cups.

Keywords: Soft robotic hands, Force sensing, Position sensing, Force control.

The originality of this thesis has been checked using the Turnitin Originality Check service.

Preface

The thesis was conducted in the Intelligent Robotics research group at Aalto University. In the nine months in Helsinki, I had a chance to work in an exciting environment around kind and intelligent people. I want to thank my labmates for a great time together. I would like to give my sincere thanks, especially to my instructor Jens Lundell for giving me the opportunity to work on this interesting topic. I also want to thank especially my supervisor Professor Ville Kyrki for helping and supporting me during the thesis work. Finally, I want to thank Professor Jose Martinez Lastra for supporting me to finalize this thesis.

Last but not least, I want to give my heartfelt thanks to my Mom, my Dad, my family, and my friends for their support and belief in me.

Helsinki, 13.8.2019

Tran Nguyen Le.

Contents

Acronyms

ADC Analog to Digital Converter. 19

AIC Akaike information criterion. 25

BIC Bayesian information criterion. 25

EAP Electro-Active Polymer. 4

FSCA Fluidic Soft Continuum Actuator. 4

FSR Force Sensitive Resistor. 20, 21

HW Hardware. 27

LPF Low Pass Filter. 32, 33, 37, 41–43, 59

MW Middleware. 27, 32, 33

PI Proportional - Integral. 26, 36, 54

PID Proportional - Integral - Derivative. 26

PWM Pulse-Width Modulation. 31, 32, 36

RMSE Root Mean Square Error. 53–55

ROS Robot Operating System. 33–35

RSS residual sum of squares. 25

SW Software. 27

List of symbols

Symbol	Description	Unit
V_I	Reference voltage of the voltage divider	V
V_O	Output voltage of the voltage divider	V
R_E	Resistance of the extra resistor in the voltage divider	Ω
R_S	Resistance of the flex sensor in the voltage divider	Ω
R_0	Resistance of the bend sensor at 0° bending angle	Ω
R_{90}	Resistance of the bend sensor at 90° bending angle	Ω
F_m	The measured force from the sensor	N
F_i	The internal force	N
F_c	The actual contact force	N
ϕ	Feature map	
n	Number of observations	
m	Feature length	
k	Number of parameters in the model	
d	Degree of polynomial function	
$\mathbf{x}$	Feature vector	
$\mathbf{X}$	Feature matrix	
$\mathbf{y}$	Label vector	
$\mathbf{w}$	Weight vector	
$\mathbf{w_{opt}}$	Optimal weight vector	
$\mathcal{E}$	Average square error loss	
$\hat{h}$	The optimal predictor	
t	Instantaneous time	s
τ	Variable of integration (from 0 to the present time t)	s
K_p	Proportional gain	
K_i	Integral gain	
K_d	Derivative gain	
e	Error between the setpoint value and measured value	
u	Control variable	
θ	Bending angle	degree

1 Introduction

For the past several decades, robots have shown great potential. For instance, robots are nowadays used extensively in complex environments such as homes, factory floors, or even hospitals. They come in different sizes and structures to perform various tasks from simple pick-and-place tasks to sophisticated surgeries on a human. The most common type of a robot is industrial manipulator. These robots are mainly seen at automated production lines on factory floors, where they must follow a predefined set of way-points to execute pick-and-place or assembly tasks on well-defined objects. The main reason robots work well in such a setting is that the environment and the objects are fully-known in advance and persistent for most of the time. However, the real world is not a predictable production line, where all objects to be manipulated and the end-effector target are known. For this reason, most of the research on robotic grasping is aimed at solving the problem of incomplete knowledge of objects and environment.

One popular approach that is currently intensively researched is to incorporate softness into robotic systems. The concept of creating robots from a highly compliant, *i.e.*, low elastic modulus, material that can easily be stretched or distended [61] is referred to as Soft Robotics [59]. Due to the soft nature of the material, soft robots not only allow increased flexibility and adaptability for manipulating a wide range of objects but also enhance the safety when collaborating with humans [52]. These unique characteristics enable soft robots to accomplish complex tasks in medical and manufacturing fields such as helping a patient in physical rehabilitation [60], creating prostheses for those missing limbs [60], or handling fresh fruits and vegetables [4]

As compliance allows more intuitive grasping, softness is now built into robotic grippers for manipulating objects. Traditionally, to grasp with rigid hands, the knowledge of an object's properties and its location must be known in detail. Then grasp planning algorithms will generate the precise contact locations where to place each finger of the gripper to grasp the object. However, with soft robotic hands, the solution can be much simpler, more human-like, and thus perform better in handling uncertainty [27]. Despite advantages of soft robots, one of their downsides is the absence of sensing capabilities, which leads to a limited range of applications. So far soft robotic hands are often used for simple manipulation tasks such as pick-and-place which do not need a complex controller and information of the hand's configuration [15]. Due to the compliance of the body, it is non-trivial to know the hand's configuration at a specific point of time, especially when being in contact with

objects or interacting with the environment. This information is vital in grasping since it can be used to determine whether a grasp is stable and whether an object behaves as intended when grasped. Furthermore, the information can also be used together with machine learning to classify grasped objects [26] or even to perform dexterous manipulation [23]. Hence, to accomplish more sophisticated manipulation tasks, the sensing capabilities for soft robotic hands should be taken into account.

Despite extensive research in soft robotic grasping, the research on integrating sensing capabilities into soft robotic hands to achieve complex manipulation tasks is still limited. A majority of the works in soft robotics focus on the hand design [13, 55, 29, 6, 8], while some did integrate sensors into the hand but only limited to classifying objects [26] and position control [15] rather than to control the interaction between the object and the hand. The work presented in this thesis addresses the open problem on studying the interaction between the object and soft robotic hands using different sensors, *i.e.*, bend and force sensors integrated into the hands. We address the following research questions:

- How to effectively choose and integrate suitable sensors into a soft robotic hand?

- How to calibrate and characterize the sensors to extract useful information, *i.e.*, the actuator's curvature and contact force?

- How to control the interaction between a soft hand and an object using the extracted information?

The need for using sensors to study the interaction between the soft hand and the object is demonstrated by performing an experiment that is challenging enough for both traditional rigid hands and soft hands without sensing capability. One suitable experiment for this demonstration is grasping deformable planar objects. The desired outcome is for robotic hands to successfully grasp the objects without dropping or crushing them. The most important factor in this problem is indeed the grasping force. If the grasping force is too small, the gripper will drop the object. On the other hand, too big a grasping force will cause damage to the object. Although a number of works on manipulating deformable planar objects have been conducted with traditional rigid hands, the problem remains because of limitations in hardware as well as control algorithms [54]. Another approach for grasping deformable planar objects is to use soft hands. However, the objects can also be easily crushed even with soft hand when high force is used. Therefore, sensing capability is needed for the soft hand to successfully achieve the goal.

This thesis is organized as follows: Chapter 2 gives an overview about the soft robotic actuator type chosen in this work, its principle, and several existing soft hand designs. Furthermore, this chapter reviews the state-of-the-art research on integrating sensing capability into soft robotic hands and manipulation of deformable planar objects. The open problem of studying interaction between soft hands and objects is also addressed in this chapter. Chapter 3 explains the research methodology from calibrating sensors to developing the controller in order to tackle the addressed issue. Chapter 4 introduces the experimental testbed of this work. Experiments and results are presented in Chapter 5. Conclusion and possible future work are presented in Chapter 6.

2 Theoretical background

2.1 Soft Hands Design

Soft robots are usually inspired by real-world biological systems, *i.e.*, soft animals, such as octopuses, snakes, or earthworms that can move in complex environments. In order to successfully mimic the locomotion of existing animals in nature, actuation mechanisms need to be developed for soft robotic bodies. Previous research [52] suggests actuating soft robots in one of the following three ways: variable length tendon, Electro-Active Polymer (EAP), and fluidic actuation (pneumatic/hydraulic). Today, one of the most common soft robot structure is Fluidic Soft Continuum Actuator (FSCA), which is a soft, deformable structure, and fluidically actuated. Due to its characteristics such as intrinsic compliance, good manufacturability and easy customization, FSCA provides the possibility to conveniently integrate sensing capabilities into itself. Due to this benefit, the work presented here will focus on fluidic actuation in general and FSCA in specific.

2.1.1 General Principle

The general principle of a FSCA is to introduce a hollow beam where two opposing sides have different stiffnesses, as shown in Figure 2.1. The basic actuation principle
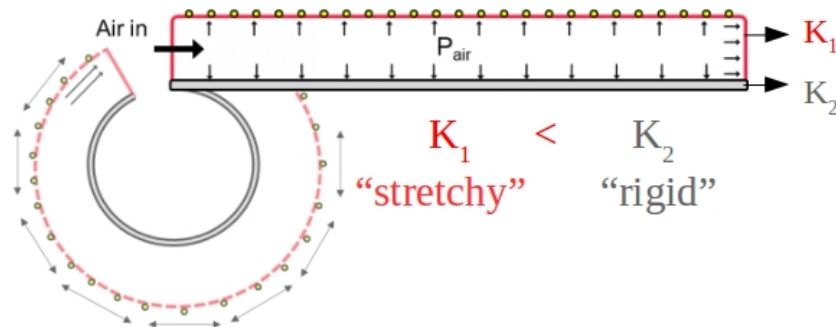

Figure 2.1 *The figure presents a lateral view of a FSCA design. A FSCA is formed by a hollow beam where the top layer has stiffness K_1, and the opposing layer has stiffness K_2. The difference in stiffness between the two layers results in the bending motion as shown in the left of the figure (Source:[17]).*

of FSCA is shown in Figure 2.2. When the hollow beam is pressurized, the entrapped fluid generates stress from inside the material, making it strain. Specifically, the side with greater stiffness elongates less than the one with smaller stiffness, causing the structure to bend toward the stiffer side [7]. The nature of this motion can
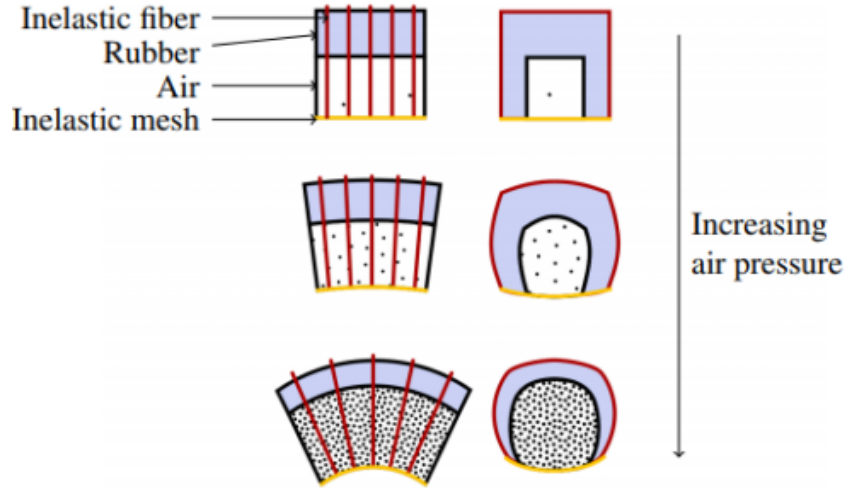
Figure 2.2 *Longitudinal cut (left) and cross-section (right) of a segment of a PneuFlex actuator when pressurizing it. Thanks to the inelastic fiber wrapped around the actuator, the rubber hull only get stretched on the top and along the main axis, causing the actuator to bend in the right direction (Source:[7]).*

be controlled by adjusting the geometry of the embedded chambers, the material properties, and the thickness of the wall. The major limitation of this structure is the ballooning behaviour of the beam as the inner chamber tries to expand in all directions when inflated. Several methods have been proposed to combat this issue such as wrapping the beam with reinforcement fabric or designing the beam in such a way that the balloon will only happen in the thinnest part, thus achieving the desired motion.

2.1.2   Existing Soft Hand Designs

As a result of new actuators and layouts, different soft hands have been developed. In this section, we will illustrate previous hand designs that acted as inspiration to the design choice used in this work.

Starfish-based Gripper

Following the pioneering soft grippers in the past, Ilievski [29] presented a starfish inspired soft gripper in 2011. The gripper comprised of three layers using embedded pneumatic networks or PneuNets. Multilayer structures, where two active layers were separated by passive layers, allowed the gripper to perform a wide range of motion. By changing the actuation strategies of the gripper, it can change its shape from concave to convex and vice versa, as shown in Figure 2.3. Moreover, the gripper incorporated a starfish-like design by placing six fingers, *i.e.*, PneuNets actuators radially around an inlet. As a result, the starfish-based gripper was claimed to
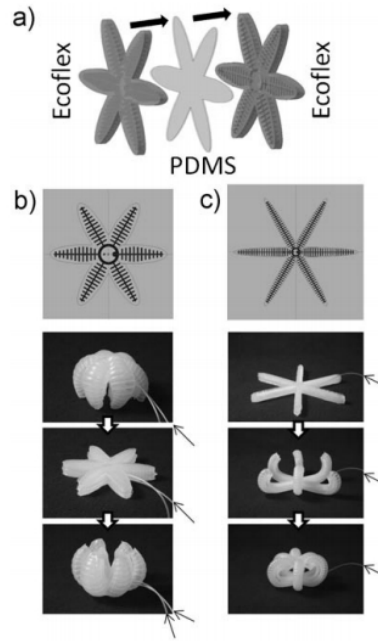
Figure 2.3 *a) Multilayer structure of starfish-based gripper. The schematic illustrates the three-layer design of the gripper, where two black layers represent two active layers, while the white layer represents the passive layer. With different actuating strategies, the gripper can change its curvature from concave to convex due to the position of the two active layers. b) The upper figure shows the top view of the gripper. The tip-to-tip diameter is 9 cm. The latter photographs demonstrate the fabricated gripper with a wide range of curvature achievable by curling upwards or downwards (from concave to convex). c) Tip-to-tip diameter is 14 cm. This starfish gripper is modified with thinner but longer arms, and capable of gripping irregularly-shaped, bigger objects. The arrows on the right of each photograph indicate tubes used for supplying compressed air for actuation (Source: [29]).*

be able to grasp objects such as an uncooked egg or anesthetized mouse without damaging it. However, the author also showed that the gripper was only capable of gripping spherical objects with a diameter of less than 10 cm and load less than 300 grams.

DRL soft hand

Another hand design was presented by Homberg in [26]. The goal of that research was to design an easy fabricated and modular soft robotic hand that is capable of grasping a wide range of objects. Subsequently, the author developed a gripper comprising of three modified PneuNet actuators that were connected to an existing robot using an interface component. The final hand seen in Figure 2.4 have two fingers on one side and one on the opposite. Each finger was then connected to a
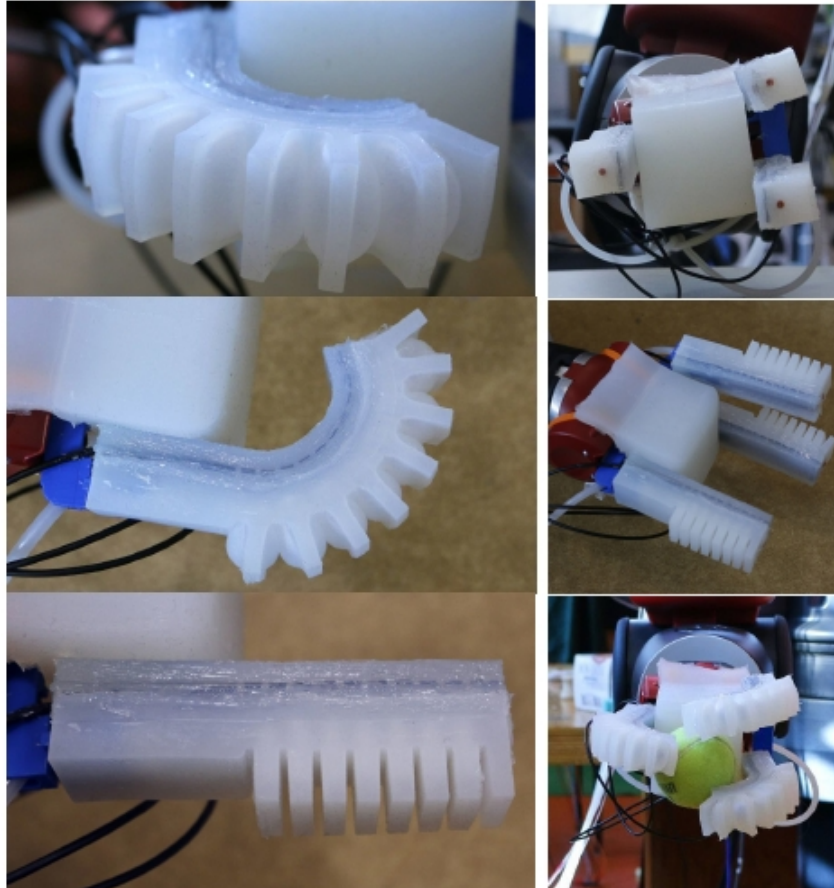

Figure 2.4 *The left figure shows one of the DRL soft hand fingers and its behaviour during actuation. The right figure shows the entire DRL hand attached to the wrist of the Baxter robot. The bottom right figure demonstrates the DRL soft hand grasping a tennis ball (Source: [26]).*

pneumatic piston, and the volume of each piston was controlled by a linear actuator. This structure, together with a block of soft material acting as a palm, allowed the hand to grasp a wide variety of objects such as a pen or a tennis ball. Moreover, the hand was equipped with a resistive flex sensor in order to obtain the curvature feedback information. The use of the sensor is detailed in the next section. After evaluating the hand with different types of grasps, the author claimed that this

structure enabled the hand to grasp from big objects such as a container of zip ties or a lemonade bottle to thin objects such as CDs or a piece of paper without damaging the objects.

RBO Hand 2

A human's hand is one of the most evolved and complex pieces of natural engineering in the human body. It not only provides us a powerful grip but also enables us to manipulate small objects with great precision. Hence, the choice of anthropomorphic design is often motivated by the goal of flexibility and dexterity of human hands [57]. In 2015, Deimel and Brock [8] developed a human-like soft robotic hand with seven fiber-reinforced pneumatic continuum actuators, called PneuFlex. The hand consisted of two parts: the fingers and the palm. Similarly to human hands, the RBO hand seen in Figure 2.5 consisted of five fingers where all of them were single PneuFlex actuators. The index, middle, ring, and little finger had identical shapes
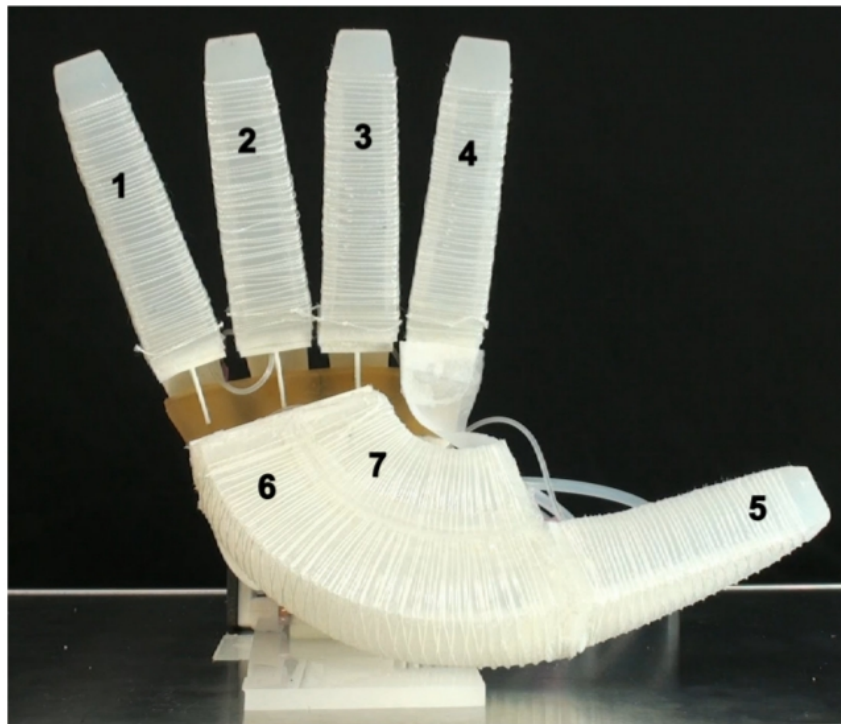
Figure 2.5 *Seven actuators of the soft anthropomorphic hand: 1 - 4 (four fingers), 5 (thumb) and 6 - 7 (palmar compound) (Source: [8]).*

while the thumb was shorter. In order to make use of the opposable thumb, the authors implemented a palmar actuator compound which comprised of two PneuFlex actuators with a circular shape. However, an exact imitation of a human's thumb required a negative curvature close to the tip, which would increase the design complexity. Therefore, the author decided to use the backside of the thumb as

primarily contact surface for pinching grasps. The hand design and its kinematics are visualized in Figure 2.5. To control the hand in a simple manner, four channels were used to actual seven actuators. The first channel drove three fingers (1,2 and 3 in Figure 2.5), the second channel controlled 4 (index finger), the third channel controlled 5 (thumb) and 7 (inner palm), and the last channel drove 6 (outer palm). To actuate the hand, industrial air valves and an off-board air supply were used. The controller of the system was based on a simple linear forward model for valve opening times to achieve the desired channel pressure, corresponding to the desired bending radius. The hand design and its control strategy were evaluated through the means of several grasping experiments. As a result, the hand succeeded in a variety of grasp postures.

2.2   Sensing capabilities enabled control of soft hands

The goal of soft robotic hands is to achieve robust grasping performance by taking advantages of material softness and mechanical compliance. These unique characteristics of the soft hand allow it to orient its surfaces to that of an object, and thus increase the contact surfaces between them. Therefore, soft hands are able to grasp objects with different shape and size without the need for expensive sensing capabilities or complex controllers. Despite the fact that soft hands are quite good in grasping a wide range of objects, a common criticism is that it is tough for a soft hand to manipulate the grasped object [25]. What if the goal is to accomplish more sophisticated tasks such as manipulating delicate objects? In order to achieve this goal, the contact force and the configuration of the hand at a specific time must be known, especially when it is interacting with the object [26]. So far, the configuration of a soft robotic hand is estimated using exteroceptive means, for instance, RGB cameras [39] or a motion tracking system [38]. In addition, these exteroceptive means are also used together with machine learning methods for teaching soft hands to learn to grasp unknown objects [5], or to perform dexterous manipulation [23].

   With the rapid development of the sensor technology, the hand's configuration can also be acquired by proprioceptive means directly attached to the hand itself. Elgeneidy [15] suggested that the sensing techniques for measuring and controlling the position of soft fingers can be divided into the following approaches: (1) make the elastomer conductive, (2) use sensors made from liquid metal, (3) use resistive flex sensors. The approaches, their advantages, and drawbacks will be discussed in the next sections.

2.2.1 Conductive elastomer

The first approach is to add different kinds of carbon content into an elastomer material to make it conductive [15]. As the material is strained, it changes its resistance, and this measurement can be correlated with the deformation of the material.

This type of sensor was encapsulated in a soft gripper, which was actuated by a linear displacement, in order to detect the presence of the grasped object, its size, and orientation [30]. The same sensor element was also embedded in another compliant gripper to control the displacement of the gripper with an adaptive neuro-fuzzy inference strategy [47].

The grand challenge of conductive elastomer sensors lies in the fabricating process of the sensor. It is extremely hard to produce a sensor with consistent electrical properties since the distribution of carbon particles inside the elastomer material can be disturbed by the actuator's repeated deformation. Moreover, it is difficult to provide a robust electrical connection. This can be a source of noise to sensory readings.

2.2.2 Sensors made from liquid metal

Recently, the use of liquid metal has enabled the development of highly stretchable strain sensors. The most common sensor of this type is the eGaIn sensor. eGaIn sensors, which shown in Figure 2.6, are made by filling inside flexible micro-channels with eutectic Indium Gallium alloy, thus the name eGaIn sensors [14]. When the eGaIn sensor is stretched, the change in the geometry of the micro-channels results in a change of resistance. This change in resistance, geometry, and pattern of the micro-channels can be used to calculate the strain or other physical parameters such as curvature [37], forces [62], and pressure [46].

This sensor was used to detect gaits in a motion-sensing suit [42]. From the robotics grasping perspective, Wall [64] introduced a method for sensorizing soft actuators using liquid metal strain sensors. The goal of the method is to produce an optimal layout from a redundant set of sensors. The layout was later integrated into the RBO Hand 2 for detection of, for example, grasp failure and slippage. In an interesting work from Morrow [43], the eGaIn sensor was attached to a soft hand to acquire pressure, force, and position control using a simple feed-forward model and PID controller. It was also used in [3] to detect the presence of a grasped object.

However, similarly to the first approach, the limitation of the eGaIn sensor is the non-repeatable process of creating flexible channels and filling the conductive
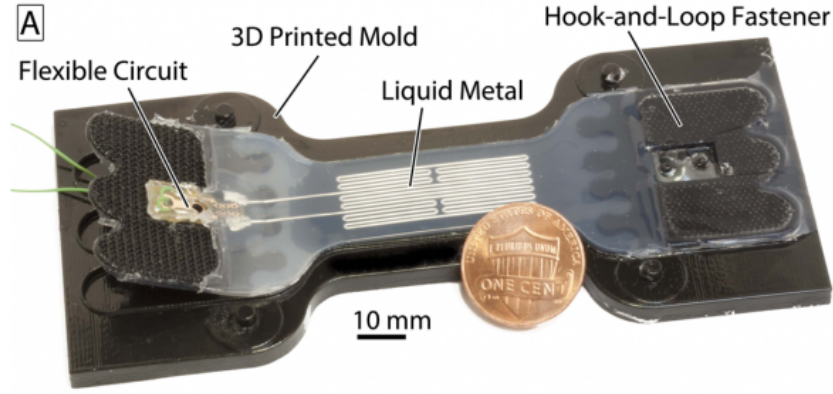
Figure 2.6 *eGaIn sensor (Source:[14]).*

liquid metal. The price of material needed for fabricating eGaIn sensor is also high. In addition, it is reported in [45] that the strain reading from this type of sensor is mostly linear and highly repeatable, but higher strain rates of the material lead to a higher unwanted hysteresis effect.

2.2.3 Resistive flex sensor

The last approach is to use commercial resistive flex sensors. The resistive sensors are made of electrically conductive patterns, placed on top of or within a flexible substrate (Figure 2.7) that can tolerate bending, vibration, thermal shock and stretching, electromagnetic interference and sensor occlusion [53]. The resistance of the sensor is changed as the resistive stripe is bent or pushed. This change can be correlated with the internal state of the finger itself. The flex bend sensor has been attached to a soft gripper for haptic identification [26]. In that work, the reading of the flex bend sensor was adopted together with machine learning algorithm for clustering the readings to distinguish the objects and based on this trained data, the grasped object can be accurately classified. Another interesting work was demonstrated by Elgeneidy [15] in an attempt to incorporate a data-driven method for predicting and controlling the position, *i.e.*, bending angle of a pneumatic-driven actuator.

The main advantage of these commercial flex sensors compared to other mentioned sensors is the simplicity, and availability of the sensors. These low-cost and simple sensors can be easily embedded in the passive layer of any soft actuators. In addition, the readings of the sensor were reported to be repeatable in both mentioned works [15, 26]. Yet, a drawback of the sensors is the consistency of the sensory measurement for different soft finger samples. The problem is indeed inevitable since the embedding process of the sensors into soft fingers is manual and the response of
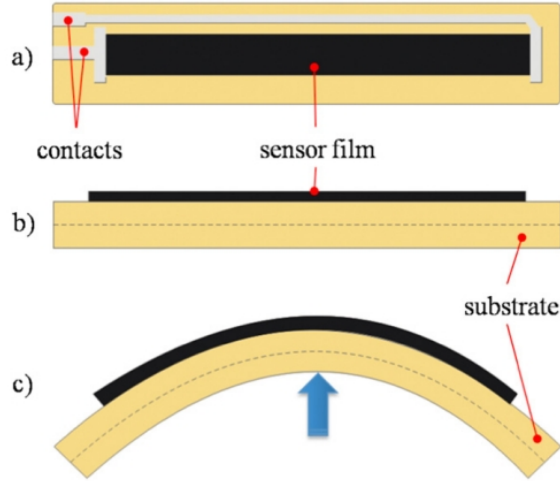
Figure 2.7 *Scheme of a resistive flex sensor. (a) Top view: electrical contacts in grey, conductive film in black. (b) Lateral view: conductive film, in black, on top of a substrate, in a lighter color. (c) Bending the substrate causes mechanical stress of the conductive pattern that leads to a change in its electrical resistance (Source:[53]).*

different sensor samples is not identical.

2.3 Manipulation of deformable objects

With over 30 years of work, manipulation of rigid objects has become a mature field in robotics. However, the research on manipulating or grasping deformable objects has not been extensively conducted in the robotics community. The main challenge is that many of the techniques, strategies and conditions such as form closure or force closure developed for the manipulation of rigid objects cannot be directly applied to that of deformable objects [54]. Thus, new approaches and methods need to be developed to achieve the manipuluation of deformable objects. However, another important challenge in developing a robotic system to manipulate deformable objects is that there are different interconnected problems to be solved. It involves the modelling of the deformable object from the deformation characteristics and the control strategy to handle the manipulation or grasping process based on the sensory feedback [33]. Another approach is to use soft robotic grippers. Unlike traditional rigid grippers, soft robotic grippers are made of highly compliant materials, thus suit better in manipulating deformable objects. The three approaches will be discussed in detail in the next sections.

2.3.1 Modelling deformable objects

One of the first works regarding the 3D modelling was proposed by Howard and Bekey [28] who developed a general solution to model and handle 3D unknown

deformable objects. In that work, the object was modelled as a network of interconnected nodes according to the Kelvin-Voigt model, which is characterized by a spring and damper in parallel. Then, by using the Newtonian equations, the deformation characteristics were calculated. As a result, the obtained information was fed to a neural network to compute the minimum force necessary to grasp the object. Another work on modelling 3D deformable objects was proposed by Lazher [36]. In that work, the deformable object behaviour was modelled by using a non-linear isotropic mass-spring system. Furthermore, a contact model was also derived in order to deal with the interactions between the manipulated body and the robotic hand fingers.

Other works on modelling 3D deformable objects incorporate vision to extract the deformation characteristics. One of those works was conducted in [35] to acquire a deformable model of elastic objects in an interactive simulation environment. Another interesting work on modelling 3D deformable objects was reported in [22] to learn models of deformable objects by physical interaction between the robot and the objects. In that work, the model parameters were derived by establishing a relationship between the applied forces and the corresponding surface deformations as observed with a depth camera. The obtained model gave the robot necessary information such as future deformations so that the robot could efficiently navigate in environments with deformable objects. The approach was evaluated by an experiment where the robot had to navigate through a curtain.

2.3.2 Manipulation of deformable objects using sensory feedback

The second problem that needs to be solved is the interaction control between the robot and the deformable objects. This requires complex sensory feedback such as force or position of the object. The mentioned feedback is usually obtained from vision and tactile sensing. Foresti and Pellegrino [21] developed a vision-based system that was capable of automatically recognizing deformable objects. The result was then used to estimate the objects' pose and to select appropriate picking points. In the case of tactile sensing, Delgado [11] presented a control strategy for grasping deformable objects, focused on elastic foams, based on tactile feedback. In that work, the relationship between the distance of the opposing fingers and the measured force from the tactile sensor, which they termed deformability ratio, was calculated. The ratio was then used to compute the maximum force to apply to an object in order to reduce the deformation of the object. The approach was later coupled with a grasp planner in [10] to create an adaptable tactile servoing control scheme that can be used in manipulation tasks of deformable objects. More recently, Kaboli [32]

presented a tactile-based framework for detecting/correcting slips and regulating grasping forces while manipulating deformable objects with the dynamic center of mass.

Some research works even study the interaction between the robotic hand and objects using the combination of vision and tactile sensing. It was reported in [33] that the feedback from vision system not only refines the knowledge about position and orientation of the objects but also provides important information to know how well the robotic hand performs the task. Hirai [24] proposed a control law to perform grasping and manipulation of deformable objects using a real-time vision system and tactile feedback. The result showed that the desired translation, rotation, and deformation of a deformable planar object could be achieved using the proposed approach. More recently, Yamaguchi and Atkeson [66, 68] proposed a vision-based tactile sensor, called FingerVision, that provided robots with a tactile sensation and visual information of nearby objects. The sensor was used in [69] to detect slippage and to develop a grasp adaptation controller that modifies the grasp to avoid slippage. Other utilities, *i.e.*, grasp failure detection, evaluation of grasp, emergency stop, and contact-event detection of the grasped object were later presented in [67]

2.3.3 Manipulation of deformable objects using soft robotic hands

Another approach to manipulate deformable objects is using soft robotic grippers. Maruyama [40] presented a gripper with fingertips constructed from a rubber bag filled with incompressible fluid. The developed gripper was later used in [44] to grasp delicate objects such as tofu. In that work, a strategy for grasping delicate objects was proposed. The proposed strategy detected the suitable grasping point where fracturing of the target object was avoided while the applied force or pressure from the fluid fingertip continued to increase. The approach was validated through several experiments on delicate objects such as tofu or potato chip. More recently, Shintake [58] developed a new soft gripper that uses electroadhesion. When voltage was applied, the gripper gently conformed to the shape of the object with electrostatic forces. After evaluating the gripper with different experiments, the gripper was seen to be succeeded in grasping objects of arbitrary shape and stiffness such as an egg, a water balloon or a piece of paper. Another soft-touch gripper was designed in [34]. In that work, the soft-touch gripper encapsulated a variable-volume chamber sealed by a thin, flexible latex membrane. An analytical model for estimating the grip force of the gripper was also developed and experimentally validated. The result showed that the developed gripper was able to grasp delicate objects such as fruits

or vegetables.

2.4   Discussion

The related research showed the importance of sensing capabilities in the manipulation of deformable objects. Without any sensory feedback it is tough to control the interaction between the gripper and the deformable object. Although many approaches have been developed to solve the problem of manipulation of deformable objects, a lack of approaches that provide versatile solutions for different deformable object types and tasks remains an open issue [54]. Another potential approach is to use soft robots. Although the sensory feedback such as contact force or position of the object is critical in solving the manipulation problem, majority of the works regarding the use of soft robotic grippers to manipulate deformable objects focus on the gripper design rather than integrating sensing capabilities into the gripper.

With the goal of developing more controllable soft robotic grippers, more research on integrating sensors into the soft body was conducted recently especially with resistive flex sensors due to the cost, the popularity and the wide-availability of the commercial sensors. Homberg has recently improved her work [26] mentioned in Section 2.2 by adding a resistive force sensor [27]. The force sensor helps to strengthen the grasp by detecting the contact between the hand and objects. As a result, the resistive bend sensor is claimed to provide valuable data which resulted in a good object identification performance. However, the force sensor provided unreliable data, which resulted in an extremely poor performance in contact detection, especially with small objects. The main reason for this problem is the position of the force sensor itself. As the force sensor was placed only at the tip at the finger, small objects such as tennis ball cannot make any contacts with the sensor even with maximum closure, resulting in no readings. While learning aspect seems to be the main interest in this work as the controller for the hand is still fairly simple, the work by Elgeneidy [15] also mentioned in Section 2.2 focuses more on the control aspect of the hand. The result of that work showed the simplicity in using empirical models and trained neural networks to predict the position of a soft actuator with only a limited dataset from inexpensive resistive sensors. Moreover, the position of the actuator was well controlled in real time using only the obtained regression model rather than complex analytical models that involve prior knowledge such as geometry or material properties of the finger. However, only position control was considered in the work. From the gathered information, studying the interaction between objects and soft hand is still considered as an open issue.

The related research showed that flex bend sensors provide reliable information. Therefore, the flex bend sensors and their characterizing techniques are potentially

adopted to this work. However, the force sensor needs to be chosen and evaluated carefully to suit the goal of this work. As stated earlier, soft hands are developed for mimicking human's grasping behaviour, *i.e.*, moulding the whole finger against the surface of the object. For this reason, placing the force sensor only at the tip of the finger is not an optimal solution for detecting contact between the hand and objects. Thus, the chosen force sensor should give the measurement along the body rather than only at the tip of the finger. With all of this in mind, this thesis will focus on studying the interaction between objects and soft robotic hands using a suitable combination of inexpensive commercial resistive sensors.

3 Research methodology and materials

The goal of this thesis is to study how complex manipulation tasks can benefit from soft robotics by incorporating sensing capabilities. This chapter briefly introduces the method behind the characterization procedure of the sensors. Data from the sensors is then used to estimate the contact force, needed to control the hand for achieving complex manipulation tasks. Finally, the concept of direct force controller is presented.

3.1 System Concept

A primitive concept of the system is designed based on the idea of utilizing sensing capabilities integrated into a soft robotic hand to achieve complex manipulation tasks. The two most important terms for this work are sensing capability and manipulation task. One of the fundamental requirements in order to successfully achieve a manipulation task is the capability of handling the interaction between the hand and the environment. The quantity that effectively represents the state of the interaction is the contact force [19]. Therefore, the system should comprise of sensors that can both describe the internal state of the finger and the contact force at each finger.

A high-level sketch of the system illustrated in Figure 3.1 consists of a sensing block, an estimation block, and a control block. In the sensing block, the characterization process of the sensor is explained. The estimation block is constructed to estimate the contact force, from which a control strategy or a controller is created to achieve certain manipulation tasks.
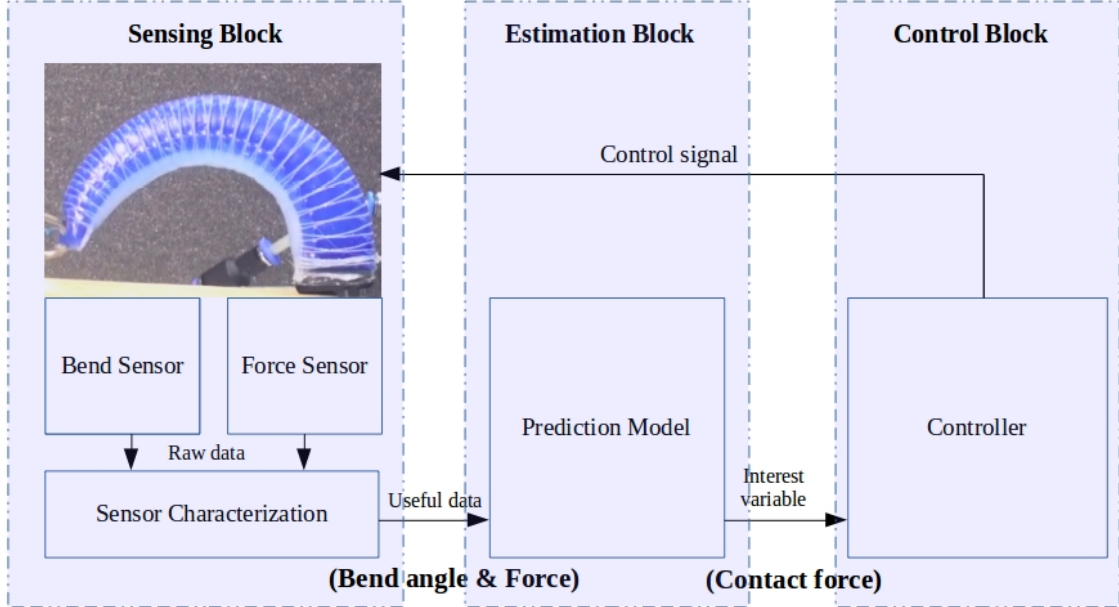
Figure 3.1 *An overview of the system. The system consists of three blocks: sensing block, estimating block, controlling block. The sensing block contains the sensor characterization process, which produces the bend angle and the applied force. The estimating block takes the output of the sensing block to estimate the contact force. The controlling block uses the estimated contact force to control the soft hand.*

3.2 Sensor Characterization

The two important quantities for achieving the goal of this work are the internal state of the finger, *i.e*, its bending curve, and the contact force. Hence, the two commercial resistive sensors used in this work are the bend sensor and the force sensor. As the direct measurements of the sensors are typically the result of the analog to digital conversion, they first need to be characterized to provide more useful data, *i.e*, bend angle, and applied force. The detail information and the characterization process of each sensor are presented next.

3.2.1 Bend sensor

The bend sensor that used in this thesis work is the Flex Sensor 4.5"[1]. This sensor is widely used in gaming, especially in virtual motion such as Nintendo Power Glove [49] and in robotics applications as robot whisker sensors [1]. In addition, it was also used in [15] for predicting and controlling the bending angle of a soft actuator.

This flex sensor is a resistive sensor. One side of the sensor consists of a layer of polymer ink which is embedded with conductive particles. Figure 3.2 illustrates the

---

[1]Flex Sensor 4.5": `https://www.sparkfun.com/products/8606`

working principle of a resistive flex sensor. Specifically, the particles provide the ink with a certain amount of resistance when the sensor is straight. When the sensor is bent away from the ink, the conductive particles move further apart, increasing the resistance. Once the sensor return to the initial pose again, the resistance also returns to the original value. Hence, the change in the resistance can be used to determine the curvature of the sensor.
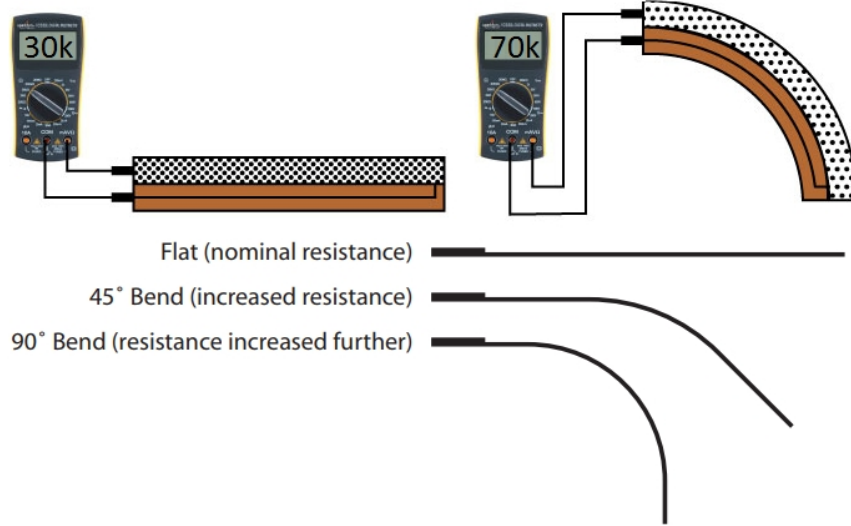

Figure **3.2** *The left photo represents the sensor when it is straight. As conductive particles are close together, the resistance is 30KΩ. The right photo shows the sensor while it is bent. As conductive particles are now further apart, the resistance increase to 70KΩ. The bottom photo shows three bending angles (0, 45 and 90 degree) of the bend sensor. These three bending angles are critical because they are used as reference points for the mapping from the resistance to the bending angle (Source: [18].*

The most convenient and simplest way to obtain data from the sensor is to connect the sensor to a microcontroller, for example, an Arduino board. The Arduino board contains an analog to digital converter. ADCs are designed to read voltage changes rather than resistance changes, thus if we want to use the Arduino board to get the readings of the sensor, we will need a way to convert the measured voltage to the sensor resistance - and a voltage divider is the easiest way to do it. The sensor is wired in series with a known resistance extra resistor to form a voltage divider, and a known voltage is applied across the divider as shown in Figure 3.3 [63]. The microcontroller's ADC is connected to the center tap of the divider so that it can measure the output voltage of the circuit using the voltage divider equation, written as

$$V_O = V_I \frac{R_E}{R_S + R_S},$$ (3.1)

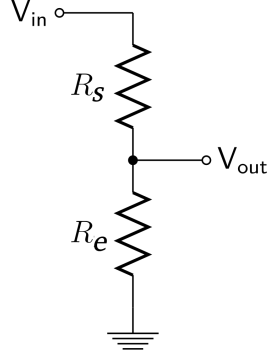where V_I is the reference voltage or input voltage, V_O is the measured output voltage,

Figure 3.3 *A simple voltage divider circuit (Source: [63]).*

R_E is the resistance of the extra resistor and R_S is the resistance of the sensor. Then the resistance of sensor can be calculated by using the formula that involves the measured voltage, the resistance of the extra resistor and the input voltage, written as

$$R_S = R_E \frac{V_I}{V_O - 1} \tag{3.2}$$

Since the bending angle is the desired output rather than the resistance, the calculated resistance was correlated to the bending angle. According to [18], the bend sensor in flat state (0° bending angle) will exhibit its nominal resistance. The sensor exhibits twofold and fourfold increases in the resistance compared to the nominal resistance with the bending angle of 45° and 90°, respectively. Therefore, the resistance across the terminals is claimed to rise linearly with the bending angle. As shown in the Figure 3.2, the resistance of the sensor at 0° and 90° bending angle can be easily measured using a digital multimeter. These values were used as reference points for mapping from the resistance to the bending angle. Thus, the bending angle of the sensor was estimated based on the measured resistance of the sensor using the formula, written as

$$R_S = \frac{R_S - R_0}{R_{90} - R_0} 90, \tag{3.3}$$

where R_0 is the resistance of the sensor at 0° bending angle and R_{90} is the resistance of the sensor at 90° bending angle.

3.2.2 Force sensor

As stated in the previous section, the force sensor to be used in this work should provide the measurement along the body of the finger rather than at the tip. To meet this requirement, a strip force sensitive resistor (FSR) was chosen. Force sensitive resistors are designed for measuring the presence and relative magnitude of localized

physical pressure [20]. They come in different sizes, shapes, and sensing ranges. To suit the purpose of our need, a rectangle shape force sensor shown in Figure 3.4 was selected.
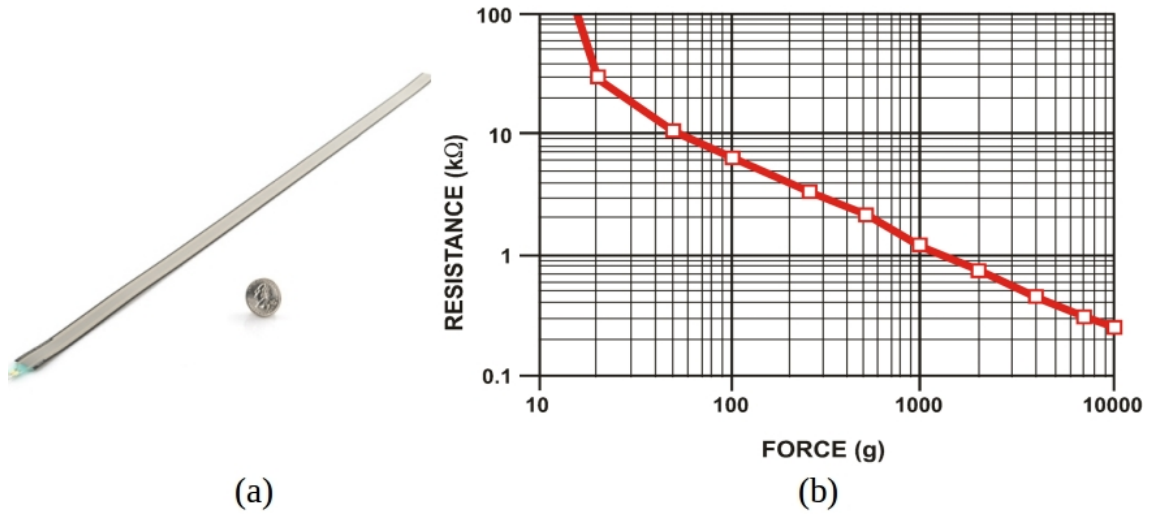

(a)　　　　　　　　　　　　　(b)

Figure 3.4 *Figure (a) shows the rectangle shape force sensitive resistor. The applied pressure can be sensed along its body. Figure (b) presents the typical force-resistance relationship. The relationship is generally linear from 50g and up, but the relationship below 50g is much steeper, and even more so below 20g. These sensors have an active threshold, i.e., a force that must be present before the resistance drops to a value below 10k, where the relationship becomes more linear (Source: [20]).*

The working principle of FSR is quite similar to the previously introduced flex bend sensor. The resistance of an FSR varies as the force on the sensor increases or decreases. The resistance of an FSR remains high when no pressure is being applied. The harder the force is applied on the sensors active area, the lower the resistance between the two terminals drops.

Similarly to the flex bend sensor, a voltage divider was used to connect the force sensor to the same microcontroller. The resistance of the force sensor was also calculated using Equation 3.3. As the desired output of the sensor is the applied force, the calculated resistance was correlated with the actual applied pressure using the resistance-force relationship graph shown in Figure 3.4.

After conducting experiments to evaluate the characteristics of the force sensor (Section 5.1), a downside of this sensor was found. Specifically, the sensor produces force measurements when it is bent in free space even without any contacts with objects or the environment. In other words, the force sensor gives the contact force even when there are no active contacts. This raises a problem in acquiring the correct value of the contact force when the sensor is actually in contact with objects.

Therefore, we will next present our solution to the problem which uses regression to estimate the actual contact force between the sensor and objects.

3.3 Contact force estimation

3.3.1 Problem formulation

Contact force is one of the most crucial variables in quantifying the interaction between a robotic hand and an object. As mentioned in Section 3.2.2, an FSR is used to measure the force that is applied to the finger. Theoretically, this sensor should directly provide the contact force between the finger and the object. However, as the sensor bends in free space (without any contact with objects), its reading continuously increases. From this point on, to make it easier to understand, the quantity of force that is caused by bending in free space will be referred to as internal force and force caused by objects as external force. Hypothetically, the real force measurement comprises of both internal force and the external force (or actual contact force). Thus, the actual contact force is assumed to be the difference between the real force measurement and the internal force, written as

$$F_c = F_m - F_i, \tag{3.4}$$

where F_c is the actual contact force, F_m the measured force, F_i the internal force.

Based on this assumption, we propose a method for estimating the actual contact force which comprises the following two steps:

1. Learning the internal force when the finger bends in free space.

2. Estimating the actual contact force from the real reading by subtracting from it the estimated internal force.

3.3.2 Learning the internal force caused by bending

Since the force sensor gives the force readings as the finger bends, it is safe to claim that the internal force heavily depends on the curvature of the finger. This can be framed as a simple regression problem where the internal force can be predicted based on the bending angle of the finger. Figure 3.5 suggests that the relationship between internal force and bending angle of the finger is non-linear. Therefore it is useful to consider a hypothesis space constituted by non-linear functions. One of
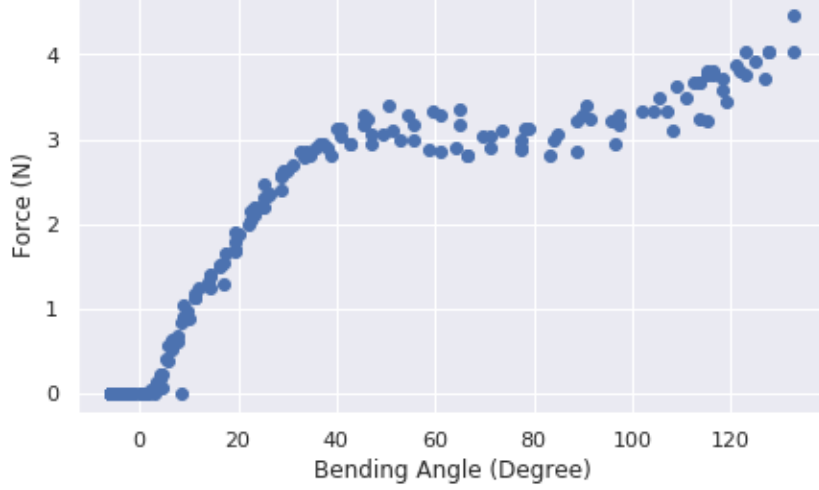
Figure 3.5 *This figure shows the relation between the bending angle and the force readings when the finger bends in free space without touching any objects.*

the most basic non-linear functions are polynomial functions [31]

$$\mathcal{H}_{\text{poly}}^{(d)} = \{h^{(\mathbf{w})}(\cdot) : \mathbb{R} \to \mathbb{R} : h^{(\mathbf{w})}(x) = \sum_{r=0}^{d} w_{r+1}x^r, \text{ with some } \mathbf{w} = (w_1, \dots, w_d)^T \in \mathbb{R}^d\},$$

(3.5)

where the hypothesis space $\mathcal{H}_{\text{poly}}^{(d)}$ is parameterized by d which is the maximum degree of the polynomial functions. As in linear regression, the quality of a predictor $h^{(\mathbf{w})}$ is measured by the squared error loss. With n data points $(x^{(i)}, y^{(i)})$, the average square error loss is calculated with

$$\mathcal{E}(\mathbf{w}) = \frac{1}{n} \sum_{i=1}^{n} (y^{(i)} - h^{(\mathbf{w})}(x^{(i)}))^2,$$

(3.6)

where $h^{(\mathbf{w})}(x) = \sum_{r=0}^{d} w_{r+1}x^r$. The goal is to find the optimal predictor $h_{\text{opt}}(\cdot)$ in $\mathcal{H}_{\text{poly}}^{(d)}$ where

$$h_{\text{opt}}(\cdot) = \underset{h^{(\mathbf{w})} \in \mathcal{H}_{\text{poly}}}{\operatorname{argmin}} \mathcal{E}(\mathbf{w}).$$

(3.7)

In order to simplify the problem, the polynomial regression is interpreted as a combination of a feature map (transformation) and linear regression [31]; that is, any polynomial predictor can be written as a concatenation of the feature map

$$\phi(x) = (x^d, .., x^1, x^0)^T \in \mathbb{R}^d.$$

(3.8)

and a linear map $g^{(\mathbf{w})}\colon \mathbf{x} \rightarrow \mathbf{w}^T\mathbf{x}$, resulting in

$$h^{(\mathbf{w})}(x) = g^{(\mathbf{w})}(\phi(x)). \tag{3.9}$$

Specifically, the feature "x" (bending angle) is first mapped to a higher dimensional feature space using the feature map. This feature map takes the original feature $x^{(i)} \in \mathbb{R}$ (bending angle) as input and returns a new feature vector $\mathbf{x}^{(i)} = \phi(x^{(i)}) \in \mathbb{R}^n$ of length $m = d + 1$ where d is the maximum degree for the polynomials in $\mathcal{H}_{\text{poly}}^{(d)}$. The resulting transformed feature vectors have the following form

$$\mathbf{x}^{(i)} = \phi(x^{(i)}) = ((x^{(i)})^d, \dots, x^{(i)}, 1)^T \in \mathbb{R}^d$$

Then, simply plugging Equation 3.9 into Equation 3.6, the polynomial regression is turned into a linear regression problem with feature vectors $\mathbf{x}^{(i)}$. To ease the representation of the regression problem of the whole dataset, the matrix and vector representations of the feature vectors $\mathbf{x}(i)$ and labels $y(i)$ contained in the dataset are introduced. In particular, we stack the labels $y(i)$ and the feature vectors $\mathbf{x}^{(i)}$, for i = 1, . . . , n, into a label vector $\mathbf{y}$ and feature matrix $\mathbf{X}$ as follows

$$\mathbf{X} = (\mathbf{x}^{(1)}, ..., \mathbf{x}^{(n)})^T \in \mathbb{R}^{n \times m}, and\ \mathbf{y} = (y^{(1)}, ..., y^{(n)})^T \in \mathbb{R}^n,$$

where n is the total number of data points in the dataset and m is the feature length. As a result, an optimal weight vector $\mathbf{w}_{\text{opt}}$ which solves (3.7) can be obtained using the equation

$$\mathbf{w}_{\text{opt}} = (\mathbf{X}^T\mathbf{X})^{-1}\mathbf{X}^T\mathbf{y},$$

Finally the obtained optimal weight vector is used to construct an optimal predictor $\hat{h} = \mathbf{w}_{\text{opt}}^T\mathbf{x}$. Thus, this estimator $\hat{h}$ with the bending angle input will be used to predict the internal force for the non-contact case when the finger bends in free space. The formula to predict the internal force caused only by bending is written as

$$F_i = \hat{h}(\theta), \tag{3.10}$$

where F_i is the predicted internal force, $\hat{h}(\theta)$ the force predictor function of θ the bending angle of the finger.

The approach of combining linear regression and feature map to solve polynomial regression allows the flexibility in the implementation and testing. In particular, different polynomial models can be quickly evaluated and compared just by adjusting the dimensionality of the feature map.

Model selection

As stated above the interest model for learning the internal force is the polynomial function of the bending angle. For polynomial models, it is critical to determine the degree of the polynomial. In general, the more parameters there are in the polynomial model, the higher the fitting accuracy is. The main reason is that the high degree polynomial model tries its best to fit the collected data precisely rather than studying the underlying distribution. Therefore, the model may fail to fit additional data or to predict future observations reliably. This phenomenon is called overfitting in the machine learning literature [12], and it is not desirable. To tackle this issue, the Akaike information criterion (AIC) and Bayesian information criterion (BIC) were developed. Both BIC and AIC attempt to solve the overfitting problem by introducing a penalty term for the number of parameters in the model [2]. As the penalty term is larger in BIC than in AIC, BIC tends to favor the lower dimensionalities [56]. Since a lower dimensionality helps to reduce the computation time, only BIC is focused from this point on.

The BIC is formally defined according to [65] as

$$BIC = \ln(n)k - 2\ln(\hat{L}), \tag{3.11}$$

where $\ln(\hat{L})$ is the log-likelihood, measuring the goodness of a fit, n is the number of observations, and k is the number of parameters of the model. In terms of the residual sum of squares (RSS) the BIC is defined as

$$BIC = n\ln(\frac{RSS}{n}) + k\ln(n), \tag{3.12}$$

The best model is the one that minimizes Equation 3.12. Thus when comparing different polynomial models, the one with the smallest BIC value is preferred.

3.3.3   Estimating the actual contact force

In the previous section, we derived the model to predict internal forces in free space bending and non-contact cases. Here, we estimate the actual contact force from the real measurement and the predicted internal force using the hypothesis proposed in Section 3.3.1. A general formula for calculating the estimated contact force is now written as

$$F_c = F_m - F_i = F_m - \hat{h}(\theta), \tag{3.13}$$

where F_c is the estimated contact force, F_m the measured force, F_i the predicted internal force and $\hat{h}(\theta)$ is the force predictor function that depends on the bending angle θ.

This hypothesis will later be studied through the means of an experiment detailed in Section 5.4.

3.4 Force controller

To interact with objects, in this case, to grasp objects, it is crucial to have a controller that receives and determines necessary contact forces to make the hand open or close in the desired manner. For this purpose, a simple direct force controller was developed, utilizing the estimated contact force obtained from Equation 3.13.

Basically, a direct force controller is a force-feedback controller attempting to maintain the desired force. The most common type of control loop feedback mechanism in the control system is the Proportional - Integral - Derivative (PID) controller. The overall PID control function is expressed mathematically according to [48] as

$$u(t) = K_p e(t) + K_i \int_0^t e(\tau)d\tau + K_d \frac{de(t)}{dt}, \tag{3.14}$$

where K_p, K_i, K_d, all non-negative, denote the coefficients for the proportional, integral, and derivative terms respectively, u(t) is the control variable, e(t) denotes the error value, which is the difference between the setpoint value and measured value, t is the time or instantaneous time (the present), τ is the variable of integration (takes on values from time 0 to the present t). As can be seen from the equation, the three gains are significant since they directly affect the system behaviour. However, the derivative action is seldom used in practice as it is sensitive to noise [16]. Since the force measurement of the force sensor is usually noisy, the derivative action is neglected. Thus, only a Proportional - Integral (PI) controller is used, mathematically expressed as,

$$u(t) = K_p e(t) + K_i \int_0^t e(\tau)d\tau \tag{3.15}$$

According to the equation, the PI controller takes the difference between the desired force and the measured force and multiplies it with a proportional gain. The error is also integrated and multiplied with an integral gain. Subsequently, the two values are added to form output, and this output will be used for commanding the hand to open or close to reach the desired force. The influence of the controller gains on the controller performance will later be presented through an experiment detailed in Section 5.7

This direct force controller scheme is simple yet provides an effective way to study the interaction between the hand and objects as the desired force is specified directly as the input.

4 Testbed

The experiments outlined in this thesis (Chapter 5) were evaluated on a soft robotic hand and a corresponding controller platform. This chapter describes the Hardware (HW), Middleware (MW), and Software (SW) used to realize the experiments. The HW setup consists of a soft robotic hand and a controller platform. The MW involves available robotics framework and communication packages. The SW part consist of the selected software architecture and corresponding implementation. The complete testbed is capable of force sensing and control of a soft hand.

4.1 Hardware

4.1.1 Soft Robotic Hand

The soft hand is designed based on the following requirements:

- Ease of fabrication and modification.

- Ability to attach different sensors.

- Capability of grasping a wide range of objects.

Achieving these requirement requires a methodological approach to selecting the actuators and the kinematics of the hand. As presented in Section 2.1.2, a number of soft hands have been developed throughout the years. Each has its own advantages and disadvantages. After evaluating the existing soft hands, several points are highlighted as follows:

- The DRL soft hand consists of three PneuNet actuators. The kinematics of the hand (shown in Figure 2.4), which resembles that of the commonly used three-finger adaptive gripper, allows the hand to grasp a wide range of objects. Additionally, it has already been encapsulated with different types of sensor to perform grasping tasks [26, 27].

- The RBO Hand 2 is made from seven fiber-reinforced actuators, which are easier to fabricate compared to PneuNet actuators. In addition, the fiber-reinforced actuator can easily be modified to withstand higher pressure by wrapping additional reinforcement helix around the actuator. Its anthropo-morphic design provides the capability of dexterous grasping (shown in Figure 2.5). However, one downside of this design is the negative curvature of the

thumb. In other words, the backside of the thumb is the primary contact surface rather than its front side. This raises the problem of attaching sensors to the thumb.

To produce a soft hand that satisfies the requirements, the advantages of two candidates, that is their ability to grasp a wide range of objects, is kept while their disadvantages, the flaw in their kinematics, should be replaced. As a result, the developed soft hand is the combination of the DRL hand and the RBO Hand 2. The hand consisted of three individual fiber-reinforced actuators acting as fingers. The kinematics of the developed hand is inspired by the DRL hand, in which two fingers are on one side, and one finger is on the opposite side. The manufacturing and sensory integrating process are detailed later. Figure 4.1 shows the final soft hand used in the experiments.
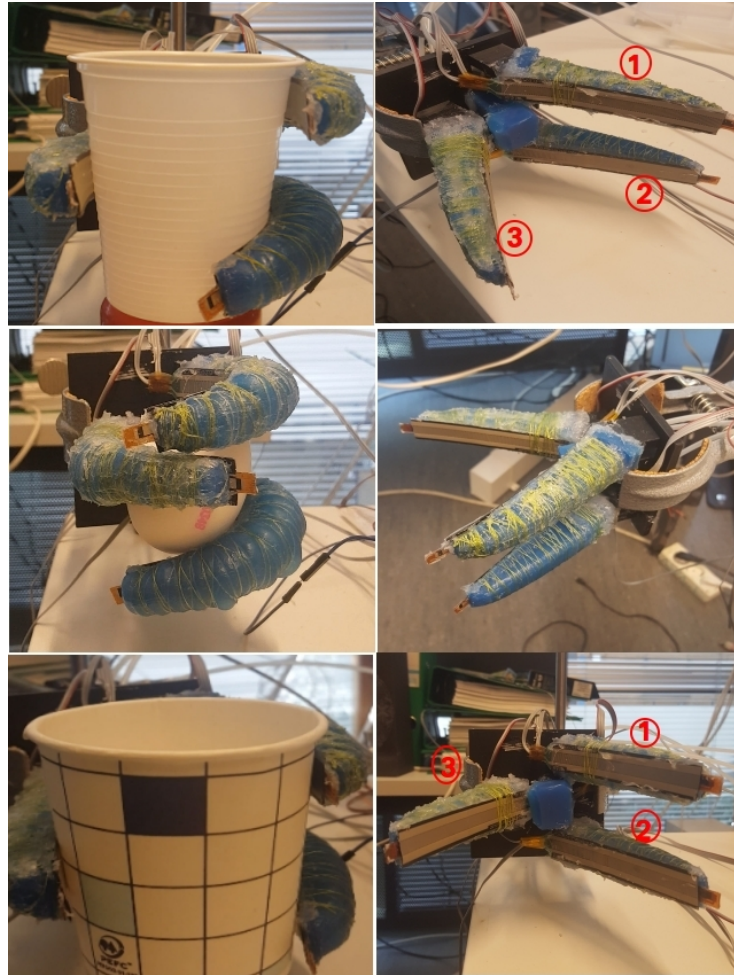

Figure 4.1 *The left side of the figure demonstrates the developed soft hand successfully grasped an empty plastic cup, an empty eggshell and an empty paper cup. The right side of the figure presents a different view of the entire soft hand. Three fingers of the hand are numbered to ease the latter representation.*

Manufacturing process

To fabricate soft actuators for the hand, we followed the steps of the manufacturing process presented in [8], which were illustrated in Figure 4.2. The process began
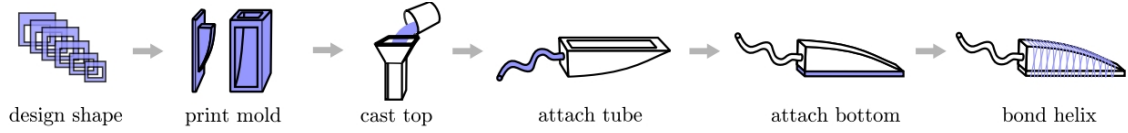

Figure 4.2 *Manufacturing steps for making a fiber-reinforced actuator (Source:[8]).*

with 3D printing a set of designed mold parts using PLA filament. Since the RBO Hand 2 actuator was chosen, the 3D models of the molds for creating the actuator were obtained from [9]. Then we prepared the Dragon Skin 10 silicone by mixing equal volumes of the provided components. The mixed material was then placed in a vacuum chamber for degassing. This extracts trapped air bubbles that could create weak spots along the actuator body. Then the top part (active layer) was cast using the printed mold and addition-cure silicone. Once the silicone was cured, the top part (active layer) of the actuator was unmolded. Next, a nylon tube was inserted at a suitable position into the active layer. The tube was responsible for supplying air to the actuator. Afterward, the air chamber was closed by placing the active layer on a thin woven sheet of polymer fabric (passive layer). Then, a PET thread was wound around the actuator in the form of a double helix to tackle the ballooning behaviour of the actuator. Finally, to keep the thread in place, a thin layer of addition-cure silicone was applied to the top and bottom side. This step finished the manufacturing process of a fiber-reinforced actuator. The complete finger and its dimension are visualized in Figure 4.3. The fabricated actuator is 90 mm long, 20 mm tall at its base. The finger gets narrower and flatter towards the fingertip.

Sensor integration

The body of the fabricated actuator is divided into two parts: active layer and passive layer. To keep the bend sensor in place, it was encapsulated in the passive layer, as shown in Figure 4.4. In contrast to the bend sensor, the force sensor needs to be in contact with the environment for getting the measurement. Hence, the force sensor was glued directly to the outer surface of the passive layer. Figure 4.4 shows how the sensors were integrated into the fabricated actuator.
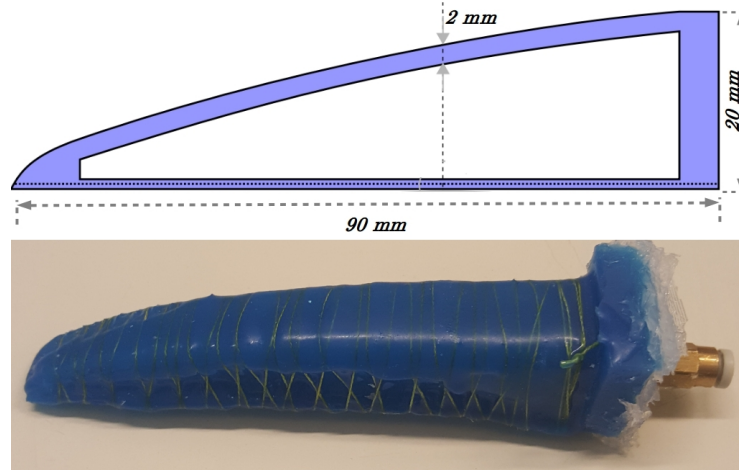
Figure 4.3 *The top figure shows the mechanical drawing of the actuator (Source:[8]). The bottom figure shows the fabricated actuator.*
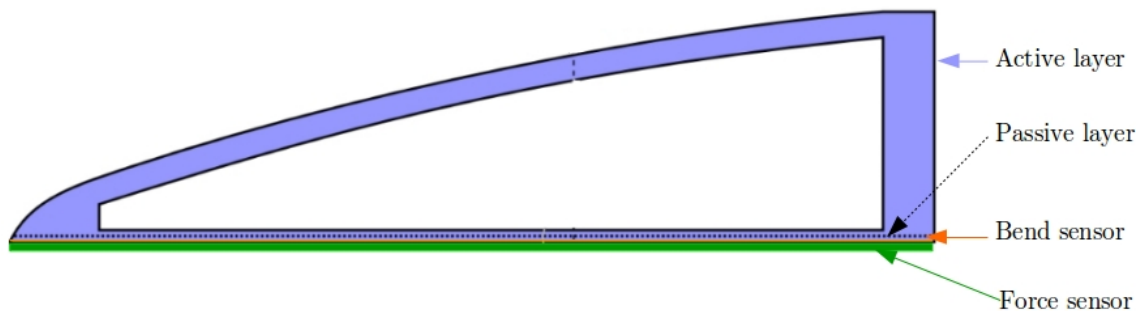

Figure 4.4 *A cross-sectional view of the actuator embedded with selected sensors. While the bend sensor (orange line) was encapsulated in the passive layer of the actuator (dashed line), the force sensor (green line) was glued to the outer surface of the passive layer.*

4.1.2   Controller Platform

To control soft actuators embedded with sensors at different operating conditions, a controller platform was constructed. Since the soft actuators used in this work are pneumatic, controlling the pressure and the duration of the input pneumatic supply is needed. The controller platform was implemented based on the proposed design by the soft robotics toolkit[1].

Controller Board

The entire controller board is visualized in Figure 4.5. The control board consists of a pneumatic regulator (which regulates the pressurized air to the system), a set of

---

[1]Fluidic Control Board, https://softroboticstoolkit.com/book/control-board

solenoid valves[2] (which can open and close to direct the flow of fluid in the system), and a set of pressure sensors[3](which is responsible for measuring the internal pressure of the system). An Arduino Mega 2560 REV3 controller is used to enable users to interface with the hardware via a serial port connection. The embedded sensors are interfaced with the Arduino controller to provide the sensors' feedback at the rate of 100 Hz. With the same Arduino controller, the board can be controlled manually (by adjusting switches and potentiometers) or automated via the programmed software.
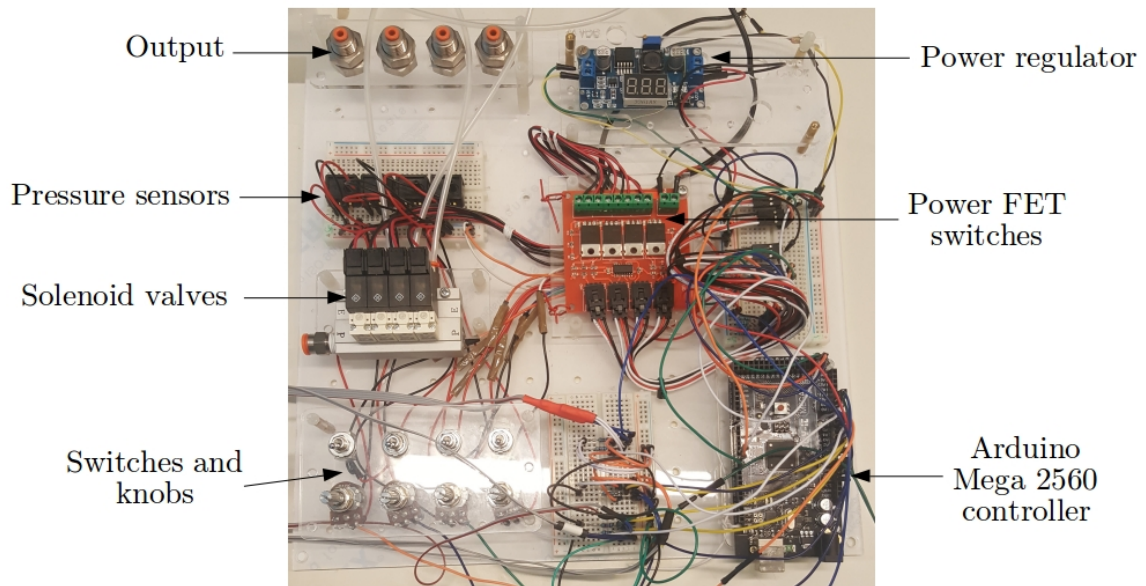

Figure 4.5 *Figure shows the developed controller board.*

The system pressure is regulated with Pulse-Width Modulation (PWM), which basically controls the opening and closing times of the valves, at a rate of 60 Hz through the Arduino board. PWM can be expressed as a technique for getting analog results with digital means. One of the most important terms in PWM is the duty cycle. The duty cycle visualized in Figure 4.6 is the proportion of 'on' time to the regular interval or 'period' of time. Duty cycle is expressed in percent, 100% being fully on, and 0% being fully off. By modulating the value of the duty cycle, analog values can be achieved. For example, the valve fully closes at 0% duty cycle, fully opens at 100% duty cycle and opens halfway at 50% duty cycle. Thus, the fixed regulated input pressure is set to the desired value based on the duty cycle of the PWM signal.

---

[2]SMC-VQ110U-5M Solenoid valve,https://www.smcpneumatics.com/VQ110U-5M.html

[3]ASDXAVX100PGAA5 Pressure Sensor, https://sensing.honeywell.com/asdxavx100pgaa5-amplified-board-mount-pressure-sensors
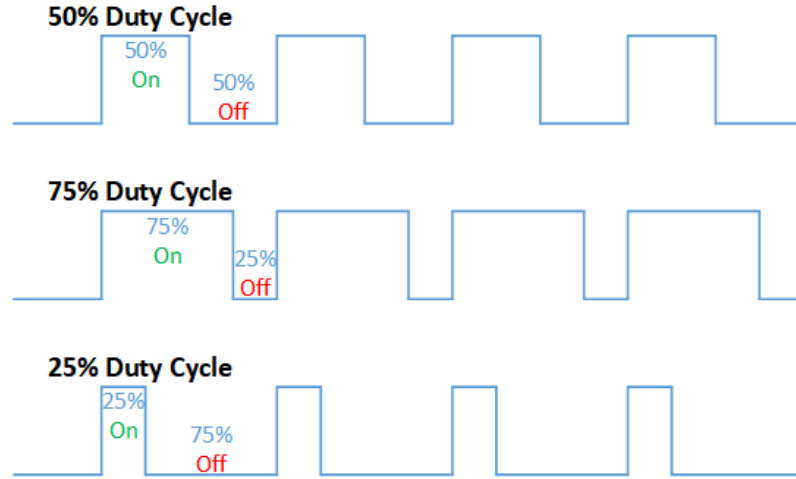
Figure 4.6 *A simple visualization for the duty cycle in three scenarios 25%, 50%, and 75% (Source: [50]).*

Pneumatic low pass filter

Although PWM provides simple and fast means for varying the pressure supply to the soft actuator, it has the disadvantage of producing non-smooth output pressure. The main reason is the mechanical switching of the high-speed valve when it is continuously opened and closed. Supplying the soft actuator with fluctuating pressure will cause vibrations in the body of the actuator, which introduces noise to the embedded sensors. Noisy sensory feedback will cause problems in the accuracy of the predictive model and the controller that use such data. To mitigate this issue, a filter was developed. One approach for designing a pneumatic Low Pass Filter (LPF) that is capable of reducing the magnitude of noise on pressure output as well as the feedback response from the embedded sensor was introduced in [41]. Figure 4.7 shows the diagram of the implemented pneumatic LPF circuit. The pneumatic LPF consists of two main pneumatic components: an adjustable volume syringe and a pipe cleaner. The syringe acts as a pressure tank (analogous to a capacitor used in electrical circuits), and the pipe cleaner acts as a pneumatic resistance (analogous to a resistor in electrical circuits). This low-cost filter setup provides the ability to fine-tune the LPF in a simple and quick manner by changing two variables: the length of the pipe cleaner and the volume of the syringe. The effect of choosing these parameters on sensory reading is discussed in more detail in Chapter 5.

4.2   Middleware

In simple terms, the middleware (MW) is a bridge between the developed software and the actual hardware. As the goal of this thesis is to control an actual soft robotic
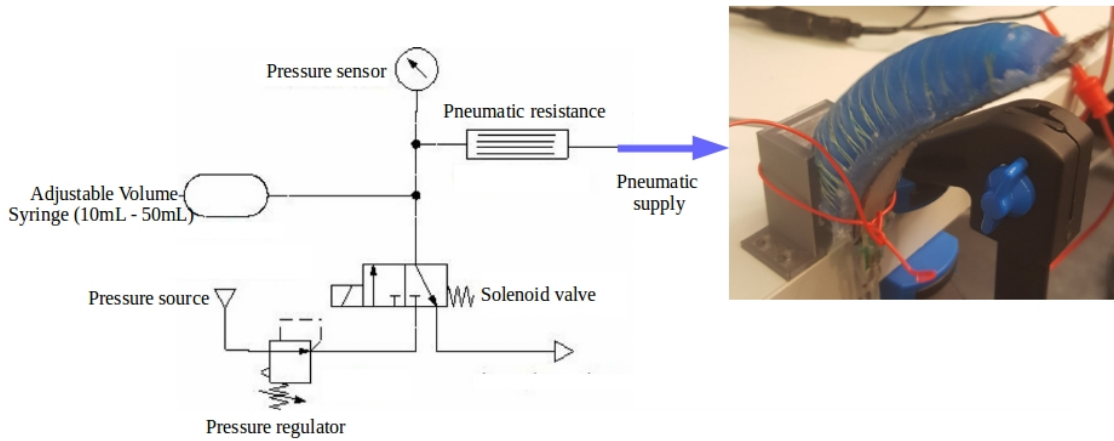
Figure 4.7 *A schematic for the pneumatic LPF controlling the actuation of a soft finger.*

hand by using feedback from the sensor, MW is utilized to serve as a communication bridge between the soft hand with integrated sensors and the user. In addition, the MW consists of a large number of already developed packages and protocols. Thus, the need for developing new code for certain problems is reduced. In this work the MW was the Robot Operating System (ROS)[4].

ROS is a framework for developing robot software. It encapsulates libraries, tools, and conventions that aim to simplify the task of creating complex and robust robotics systems [51]. ROS programs are implemented as nodes with publish-subscribe communication mechanism. These ROS nodes can communicate with each other to exchange data by sending a stream of messages with a defined type to a specific topic name [51]. Due to the publish-subscribe communication scheme, any ROS nodes within the network can retrieve the desired data by subscribing to the right topic.

As mentioned in Section 4.1.2, the embedded sensors, and high-speed solenoid valves are connected to an Arduino micro-controller. To interface the Arduino board (serial device) with ROS via a serial port connection we used the **rosserial**[5] package. **Rosserial** is a protocol for wrapping standard ROS serialized messages and multiplexing multiple topics and services over a character device such as a serial port or network socket. The communication is over a serial transmission line and uses serialization/de-serialization techniques for transmitting ROS messages. Thanks to the **rosserial** package, the sensory reading can be sent to the PC for processing and handling. Furthermore, the solenoid valves, which are responsible for actuating the soft actuator, can also be controlled by the PC through ROS.

---

[4]The ROS version was Kinetic.
[5]http://wiki.ros.org/rosserial

4.3   Software

This section is devoted to explaining the selected software architecture and implemented functions to complete the system.

Software Architecture

The whole procedure for controlling the soft hand using sensory feedback can be divided into two phases: system calibration and system operation. In the system calibration phase, we record the feedback of the sensor and learn the predictive model from the data. In the system operation phase, we process the data to estimate the contact force and control the soft hand based on the estimated contact force. This procedure is shown in Figure 4.8.
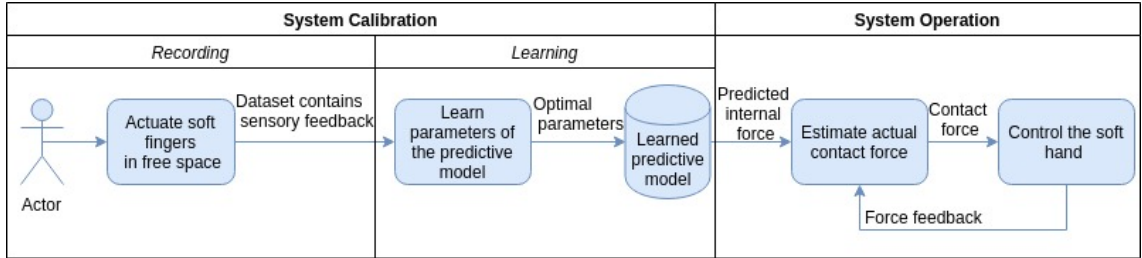

Figure 4.8 *The two phases shown in the figure need to be achieved in sequence so that the soft hand can be controlled using sensory feedback. The calibration phase, which comprises of recording and learning steps, is only done once. Meanwhile, the operation phase is executed iteratively to control the hand in the intended manner.*

System calibration phase

Record the data

As discussed in Section 3.3.2, to estimate the actual contact force between the hand and the object, the predictive model for predicting the internal force needs to be derived. For this purpose, a dataset containing the bending angle and corresponding force readings were obtained.

Firstly, the user initiates the recording phase. At this point, the sensory reading is published at the rate of 100 Hz. The data is stored in ROS bag files and will later be used for learning the predictive model. When the setup is finished, the finger is then inflated slowly by increasing the duty cycle by 2% every 200 ms. As the duty cycle reaches 90%, the finger is deflated by decreasing the duty cycle by 2% every 200 ms. As the duty cycle goes back to 0%, it starts to increase again. This cycle repeats until the user terminates the recording.

The recorded ROS bag files are then passed into a script. This script extracts and saves data of interest, *i.e.* bending angle and force, into different files. Next, all the extracted files are merged into one. As a result, one file containing the bending angles and corresponding force readings is obtained. This data is used for learning the predictive model in the next phase.

Learn the predictive model from the recorded data

The goal of this phase is to produce a model for predicting the internal force caused by bending in free space. During the learning phase, the predictive model is trained and its parameters stored for the processing and controlling phase. The training of the model is done offline by taking the obtained dataset in the previous phase as input and follows the method explained in Section 3.3.2 to learn the model. Once the predictive model is learned, its parameters are written in a text file for further purposes.

System operation phase

To incorporate the contact force estimation and the control of the soft hand in a simple manner, we implemented the functionality in a ROS node. This node was responsible for receiving sensory feedback, then iteratively estimating the contact force and controlling the soft hand according to the estimated contact force.

The workflow of the proposed control strategy is visualized in Figure 4.9. In
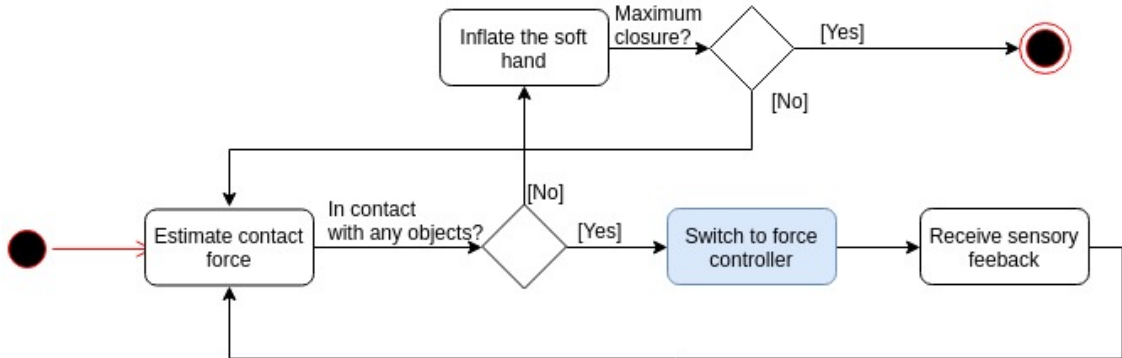

Figure 4.9 *This figure shows the workflow of the developed controller.*

particular, the sensory feedback is continuously fed to the node at the rate of 100 Hz. This information was used together with the predictive model obtained in the learning phase to estimate the contact force. If the hand does not detect any contact between itself and objects, it will continue to close until maximum closure. However, if the hand is in contact with the object, the program switches to the force controller scheme. The force controller architecture with the feedback of bending angle and

force is visualized in Figure 4.10. This force control scheme tries to keep the contact
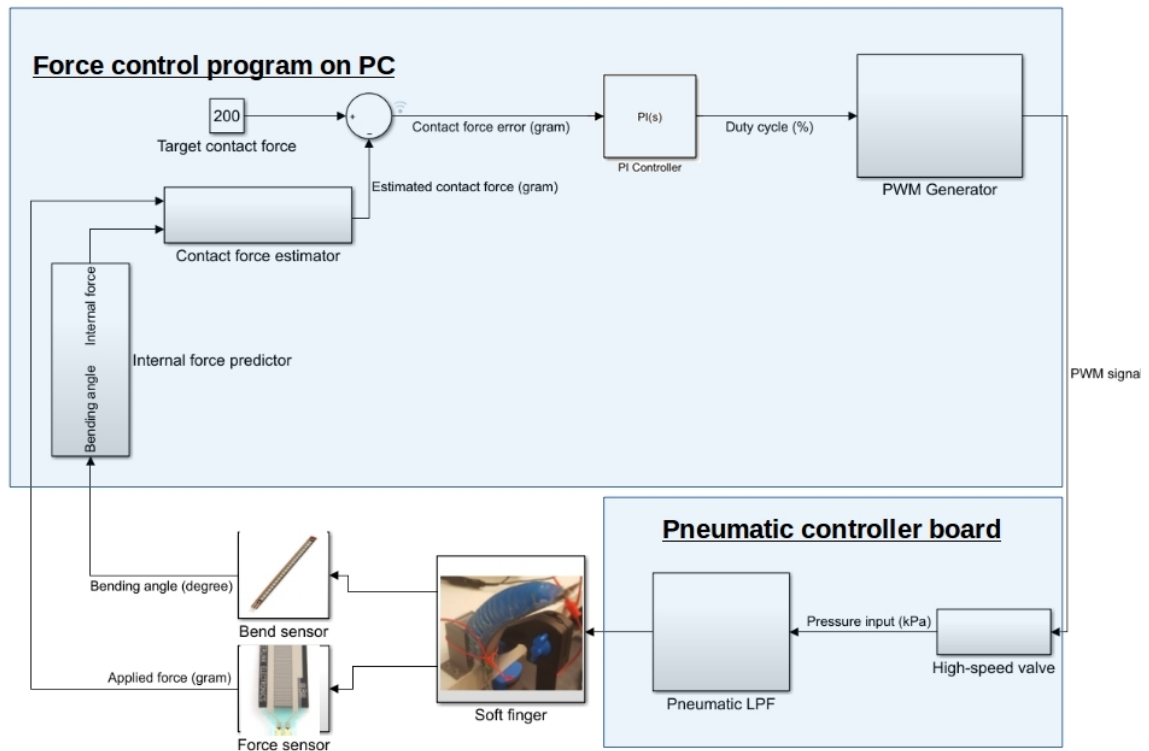

Figure 4.10 *The figure shows a schematic diagram summarizing the basic operation of the force controller.*

force the same as the desired target value using the sensory feedback. As mentioned in Section 3.4, the force controller is basically a closed-loop PI controller, which takes the difference between the current estimated contact force and the target contact force to calculate the duty cycle value of the PWM signal. Then the controller uses the new value of the duty cycle to generate the PWM signal that regulates the supplied pressure to the soft finger to achieve the desired target contact force.

5 Experiments and Results

The main questions we wanted to answer in the experiments were:

1. What are the characteristics of the embedded sensors?

2. How do the parameters of the pneumatic LPF affect the pressure signal and the reading of the sensor?

3. Is the predictive model learned from the smoothed sensory reading accurate enough to provide reliable internal forces?

4. Does the proposed hypothesis in Section 3.3.1 provide accurate contact force?

5. How can the estimated contact force be used to detect when contact between the hand and the object happens?

6. Is it possible for embedded sensors to estimate object properties such as its stiffness?

7. Can the soft hand force controller work based on the estimated contact force?

In order to provide justified answers to these questions, we conducted seven experiments. The first experiment evaluates the characteristics of the embedded sensors (Section 5.1). The second experiment examines the effect of the pneumatic LPF parameters on the pressure signal and the sensory feedback (Section 5.2). The third experiment targets the accuracy of the internal force predictive model (Section 5.3). The fourth evaluates the proposed method for estimating the contact force (Section 5.4). The fifth experiment targets the use of estimated contact force in contact detection (Section 5.5). The sixth experiment examines the use of the sensory feedback in realizing the hardness of objects (Section 5.6). The seventh experiment targets the accuracy of the proposed force controller and the effect of its controller gains (Section 5.7). The last experiment is to evaluate the proposed control strategy in grasping deformable planar objects without breaking them as this will demonstrate the need of using sensors to control the interaction between a soft robotic hand and an object (Section 5.8).

All the presented experiments were conducted on the hardware setup introduced in Section 4.1 consisting of a soft robotic hand embedded with the selected bend sensor and force sensor, and a controller platform.

5.1 Embedded resistive flex sensors characterization

5.1.1 Voltage divider

To form a voltage divider, an extra resistor was needed for the circuit. The range of the value of the extra resistor was considered carefully as it heavily affects the measurement. If the value of the extra resistor is much larger than that of the bend sensor, the extra resistor will dominate the bend sensor and vice versa. According to the dataset of the sensors, the value of the extra resistor should range from 10 kΩ to 100 kΩ. Different values of the extra resistor provide different resolution of the reading as well as different response time. It is recommended to use the 47 kΩ extra resistor as it gives good readings in reasonable response time.

5.1.2 Bend sensor

An experiment was performed to evaluate the behaviour of the flex bend sensor when it was integrated into the soft finger. In this experiment, the soft finger was inflated from 0 kPa to 60 kPa by adjusting the duty cycle (explained in detail in Section 4.1.2) from 0% to 80% with three different durations. As the duty cycle reached 80%, the finger was set to its initial position by setting the duty cycle to 0%. For each actuation duration, the experiment was repeated 35 times to evaluate the accuracy and the repeatability of the sensory reading. Figure 5.1 plots the duty cycle input against the estimated bending angle of the bend sensor when inflating the finger for three different durations. The plotted cycle shows the bending angle of the bend
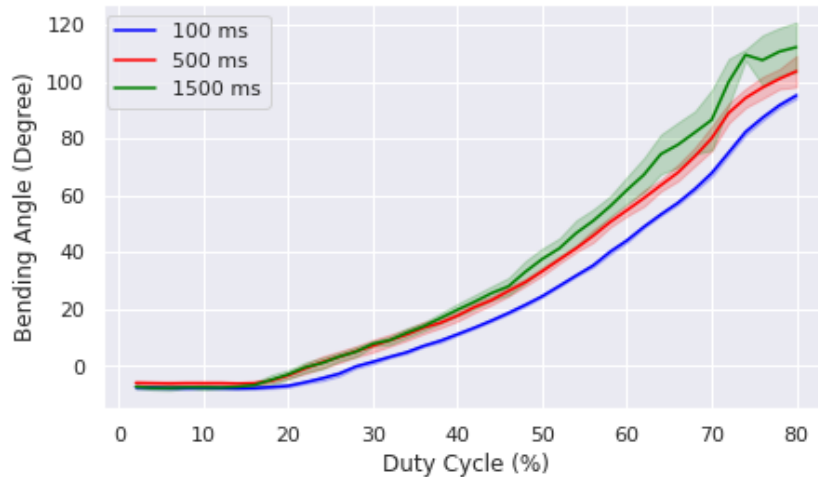

Figure   5.1 *The figure shows the bending angle against the duty cycle input for three different durations: 100 ms, 500 ms, and 1500 ms. For each actuation duration, 35 repetitions were conducted.*

sensor increasing upon actuation as the internal pressure builds up by increasing the duty cycle. The response was observed to be fairly repeatable. However, it is observed that the longer actuation duration, the more fluctuations there are in the reading. In addition, the longer actuation duration causes a systematic extension in the readings. The main reason for this extension is that during the actuation duration, the finger continues to bend rather than keeping the same position. The longer the actuation duration is, the more the finger bends which, in turn, increases the bending angle. Therefore, one can conclude that the reading of the bend sensor is slightly dependent on the actuation duration. Hence, to obtain stable readings of the bend sensor, suitable actuation duration needs to be carefully considered and selected.

5.1.3 Force sensor

To evaluate the behaviour of the force sensor, an experiment was conducted, in which certain objects were applied on the body of the sensor, see Figure 5.2. In this
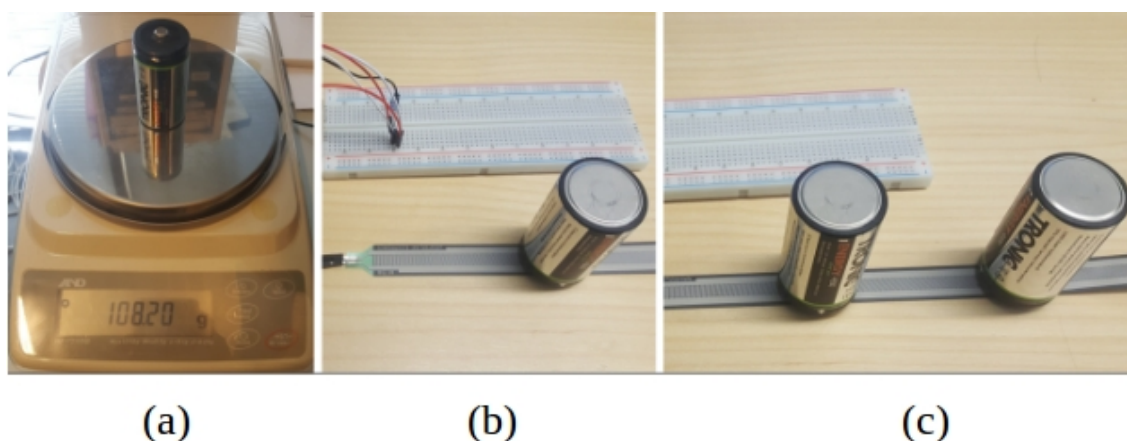

(a)   (b)   (c)

Figure 5.2 *This figure shows the experimental setup for evaluating the behaviour of the force sensor. Figure (a) shows the object (battery) that was used for the experiment and its weight (108.20 gram). At first, one object was placed on the force sensor (b) and then multiple objects were placed at different points along the body of the sensor (c).*

experiment, at first, only one object was placed on the sensor to check the accuracy of the readings. Then several objects were placed along the body of the sensor to evaluate the sensing capability of the sensor along its body. Figure 5.3 plots the force measurements at each phase of the experiment. The plotted graph shows a good result of the force measurements during the experiment. Although there are some small variations due to noise in the measurement, the readings obtained from the sensor still follow the reference value quite well. The results from the force sensor were converted from N to gram to evaluate easier. Specifically, in the case of
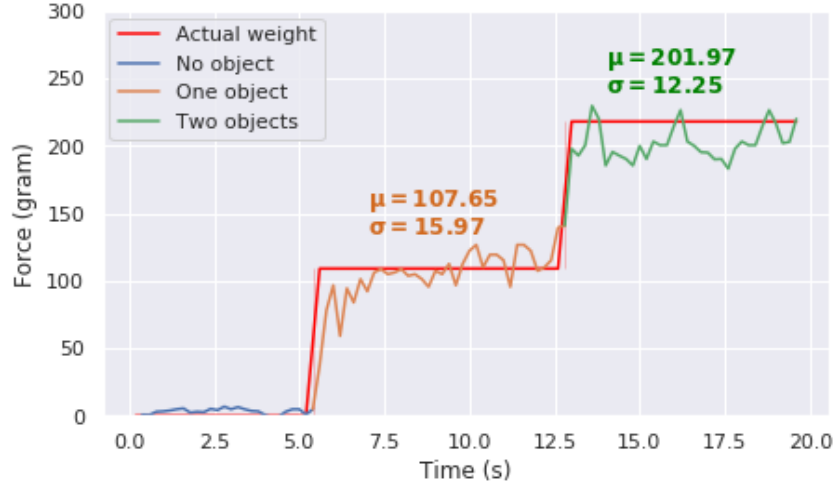
Figure 5.3 *The figure presents the force readings in each phase of the experiment. The red line represents the reference value, which is the actual weight of the object. The orange and green line represent the measured weight in the case of one object and two objects, respectively. Despite some fluctuations in the readings, the force sensor provides a reasonable result.*

one object, the force sensor produced a reported result of 107.65 g and 15.97 g (as shown in Figure 5.3) on measurement mean and standard deviation, respectively. The result is quite good compared to the ground truth force of 108.2 g. In the case of two objects, the ground truth force, the measurement mean, and standard deviation were 216.4 g, 201.97 g, and 12.25 g, respectively. The result shows that the force sensor can sense the pressure at any points along its body, and it will return the cumulative load as the final result.

At this point, the force sensor has performed well in stationary situations. However, we also need to conduct an experiment to quantitatively evaluate the performance of the same sensor integrated into the soft hand. In this experiment, the force sensor was integrated into the soft finger, which was inflated by increasing the duty cycle input by 2% every 200 ms in free space without any contacts with the environment or objects. When the duty cycle reached 80%, the finger was then deflated to its initial position by setting the duty cycle to 0%. The experiment was also repeated 35 times to observe the quality and repeatability of the force sensor. Figure 5.4 shows the duty cycle input against the estimated applied force of the force sensor after 35 repetitions. Theoretically, the estimated force should remain zero as there is no contact between the finger with any objects. However, it is noticeable that the estimated force increases when the finger is actuated, although there are no active contacts. The main reason of this behaviour stems from the fact that when the finger bends, the force sensor gives the reading at the curved point. This raises

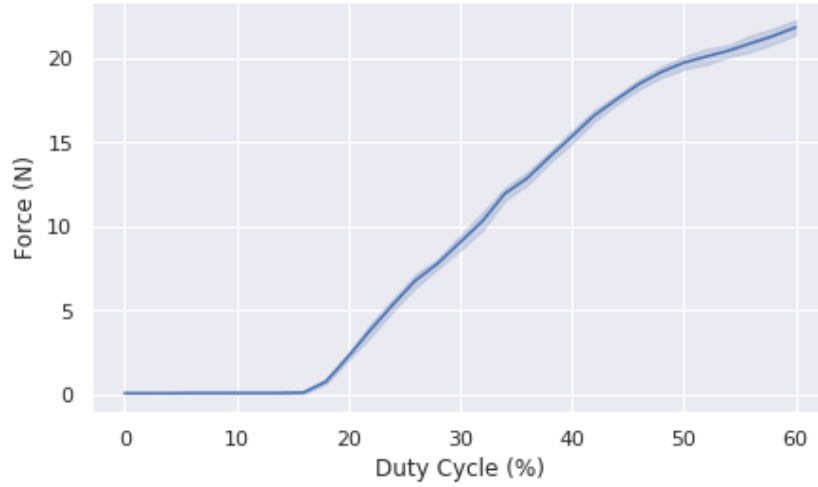a problem in acquiring the correct value of the contact force when the finger makes contact with an object.

Figure 5.4 *This figure shows that the force sensor provides the force reading even when the finger bends in free space.*

5.2 Influence of the gains of the LPF on sensory readings

As mentioned in Section 4.1.2, a pneumatic LPF was implemented to reduce the noise in the pressure signal and the sensory feedback. A two-stage experiment was conducted to examine the effect of the pneumatic LPF on the pressure signal and the readings of embedded sensors. In the first part of the experiment, a pressure sensor measuring the internal pressure was used to get the pressure feedback from the system. The soft finger was then actuated with 50% duty cycle and was maintained at that level when LPF was and was not used. Figure 5.5 shows the pressure response measured at 50% duty cycle in both cases. From the figure, one can easily observe when LPF is not applied, the pressure signal oscillates abruptly because of the switching mechanism of the high-speed valves. However, by introducing the pneumatic LPF, the pressure response is significantly improved, reducing the vibrations in the soft finger.

The second part of the experiment studies how the pneumatic LPF and its parameters affect the sensory feedback of the embedded sensors. The two tunable parameters of the pneumatic LPF are the volume of the syringe and the length of the pipe cleaner. At first, the effect of the length of the pipe cleaner on the readings was evaluated. The result showed that the sensory readings were identical for different length of the pipe cleaners. As the length of the pipe cleaner does not heavily affect the sensory feedback, we only consider the volume of the syringe, which ranges from
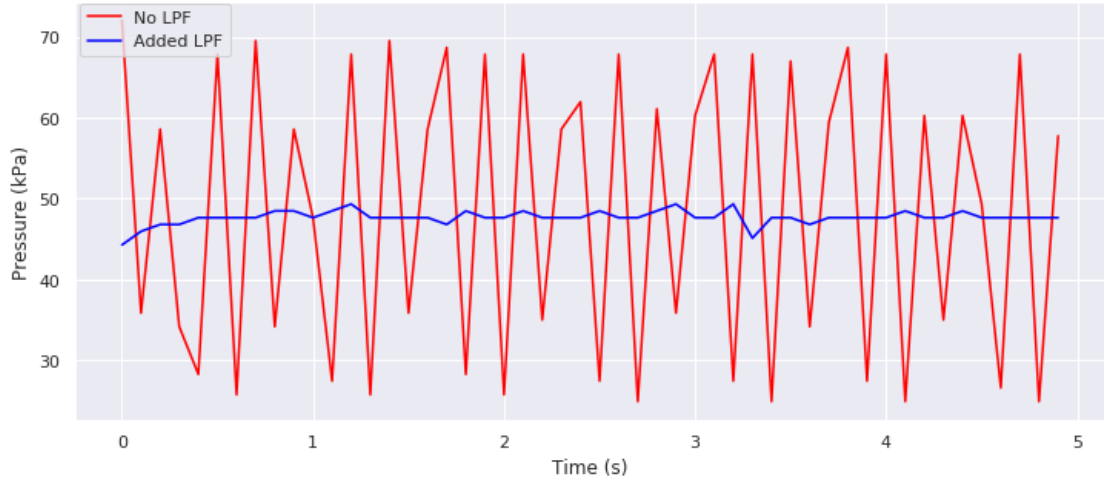
Figure 5.5 *Damping of oscillations in internal pressure measurements using pneumatic LPF.*

10 ml to 50ml. In this experiment, the soft finger was also actuated and maintained at 50% duty cycle and the reading of the force sensor was recorded in four cases: 1) no LPF, 2) 20 ml, 3) 30ml and 4) 40ml. Figure 5.6 shows the readings of the force sensor in the four cases. As can be seen in the figure, when the LPF is not applied,
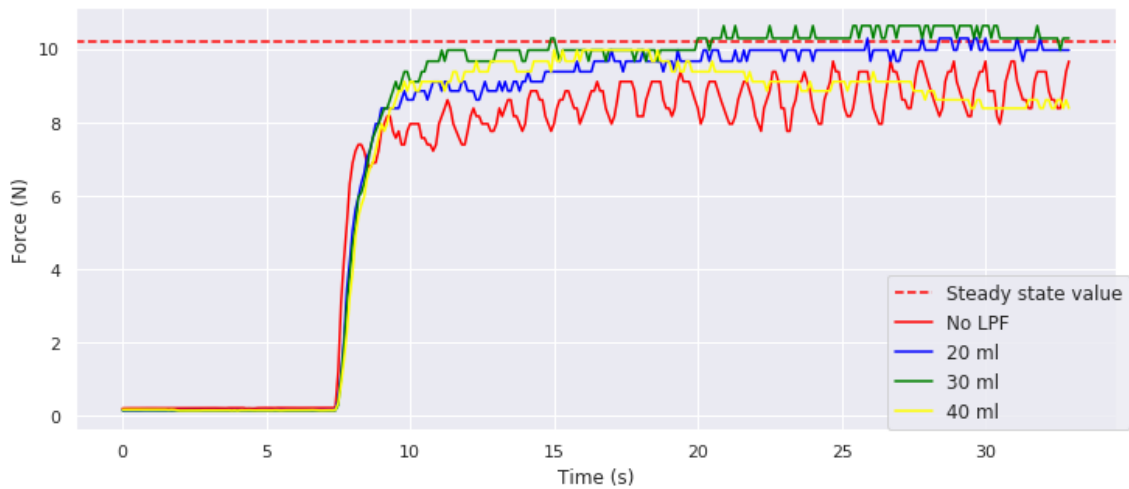
Figure 5.6 *Damping of oscillations in force sensor measurements using pneumatic LPF with different volume of the syringe.*

the soft finger vibrates, which leads to fluctuating force readings. Although the force reading is significantly smoothed when the LPF is applied, different volumes of the syringe provide different response signals. When the volume of the syringe is set to 40 ml, the response rises slowly and consequently has a high value for the rise time. It is also observed that the response, in this case, stays below the steady-state

value rather than reaching the target value. The responses in the 20 ml and 30 ml setups have a lower rise time, thus faster responses compared to that of the 40 ml setup. However, the 30 ml setup provides better and more stable response compared to the 20ml setup. Therefore, a syringe volume of 30 ml was chosen to be used in subsequent experimental evaluations. It is important, however, to avoid changing the volume of the syringe and the length of the pipe cleaner since this would heavily affect the predictive model and the controller that use the data.

5.3 Internal force predictor

With the pneumatic LPF, the sensory feedback is smooth and works better for estimating the contact force. The main problem of the force sensor is that it does not directly give the contact force between the hand and the object. As the sensor bends, it introduces force measurements even when it is not in contact with any objects, a phenomenon already discussed in Section 5.1.3 and which we referred to as internal force. To predict the internal force based on the bending angle of the finger, a predictive model, which followed the method mentioned in Section 3.3.2, was constructed. As the internal force directly affects the estimated contact force, a high accuracy predictive model is desired. The dataset used for learning the model was obtained in the system calibration phase mentioned in Section 4.3. As discussed in Section 3.3.2, to avoid the overfitting problem, the BIC was used for considering the appropriate number of parameters in the model. To do this, BIC values of different polynomial models need to be calculated. Figure 5.7 shows the BIC values of different polynomial models (from first to tenth-degree models). It is

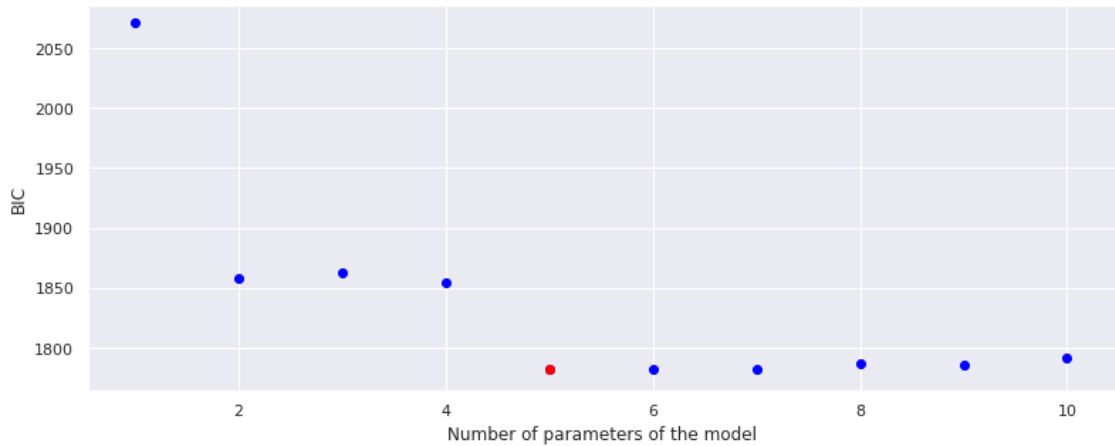***Figure*** ***5.7*** *The figure shows the BIC values of different polynomial models. The red point indicates that the fifth-degree polynomial model has the smallest BIC value.*

noticeable from the figure that the fifth-degree model has the smallest BIC value.

Therefore, the fifth-degree model is considered for further analysis. To observe how well different models fit the real data, Figure 5.8 plots different predictive models on the real dataset. From the left figure, it is noticeable that the linear model
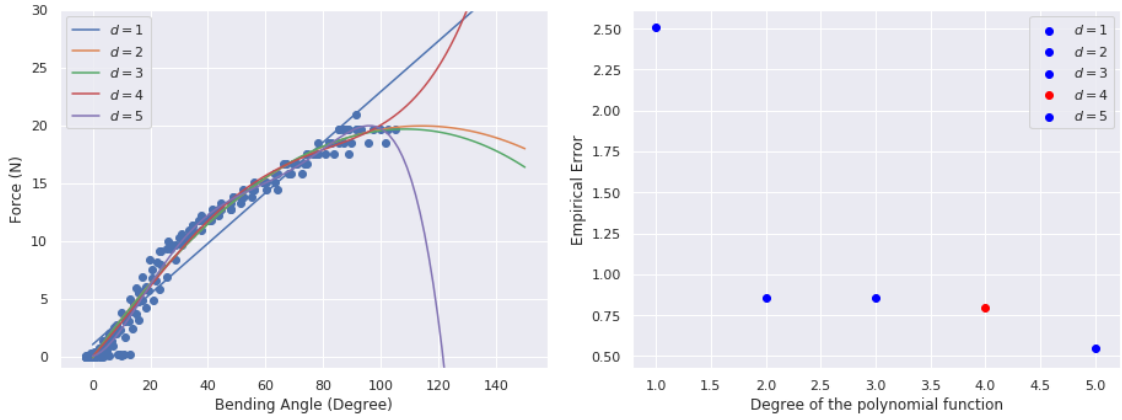

Figure 5.8 *The left figure shows different internal force predictive models from a linear model to a fifth-degree polynomial model. The right figure shows the corresponding empirical errors of the models. The red point indicates the empirical risk of the chosen model, i.e, fourth-degree polynomial model.*

(blue line) and the fourth-degree polynomial model (red line) describe the pattern of the data better than other models including the suggested model from BIC, *i.e.*, fifth-degree polynomial model (purple line), as the predicted force of the two models continues to increase after 120° bending degree. The right figure shows empirical errors of the models. Although the empirical error of the fifth-degree polynomial model is the lowest, the model does not provide logical force after 120° bending degree. Thus, the fifth-degree polynomial model was overfitted. As a result, the fourth-degree polynomial was chosen as the optimal model to predict the internal force.

Then, the accuracy of the fourth-degree polynomial model was evaluated on three different fingers of the soft hand. Figure 5.9 shows the predicted internal force against the real data and the error between the two. It is seen from the left figures that the collected data from three fingers are different from each other. The main reason for this lies in the fabricating process of the finger, and the sensor integrating process as the processes are done manually, the fingers are not identical. This, in turn, leads to the variation in the collected data. Regardless of this matter, the R^2 values show that the predictive models fit the data very well. The figure also shows the error between the real measurement and the predicted value of the internal force. The error is considered to be reasonable as it varies in the range of 0.4 N to 1.96 N of force. Due to the fluctuation of this error, a certain threshold is set to safely detect contact between the finger and an external object. The value of the threshold
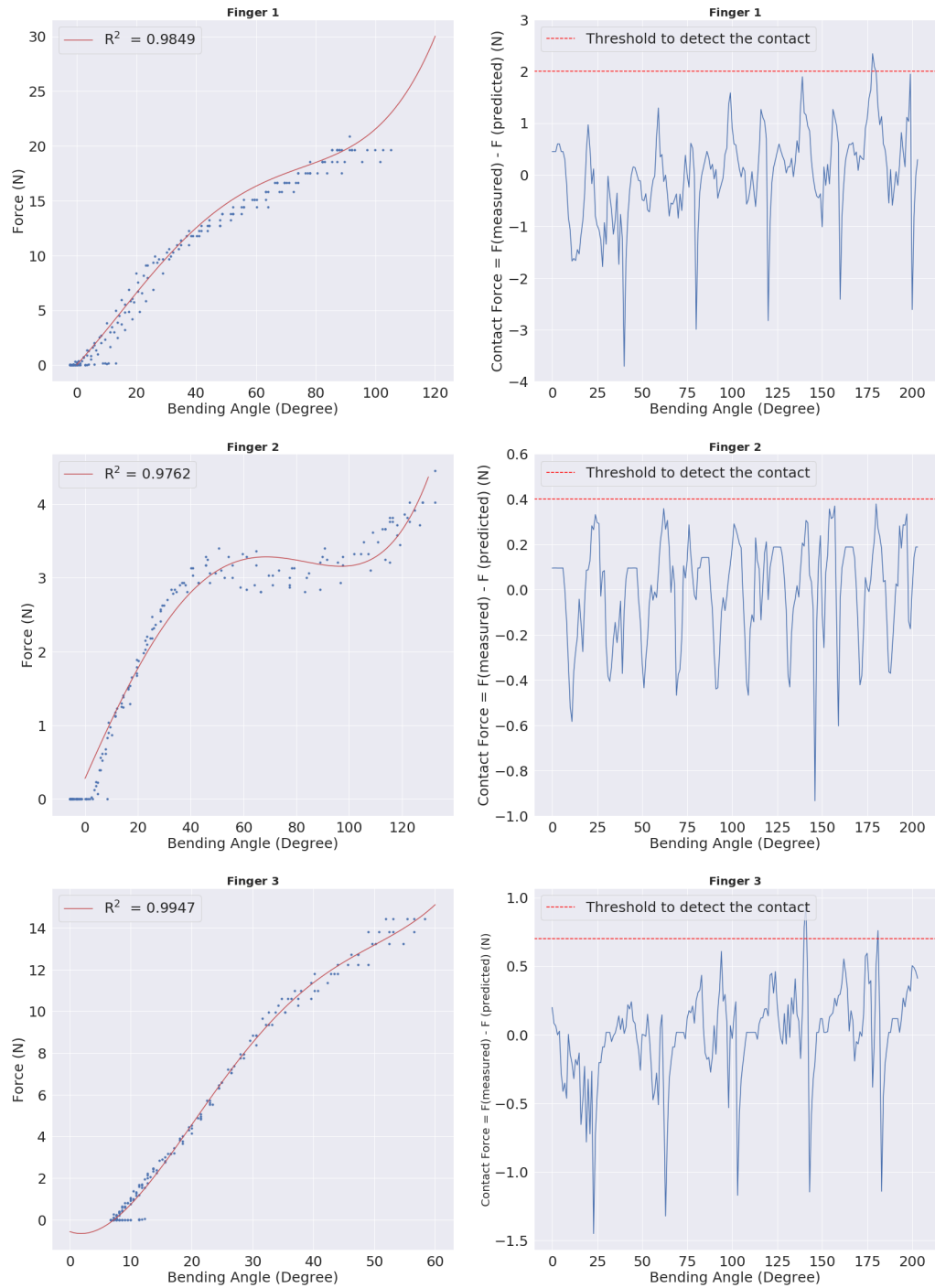
Figure _5.9_ _The left figures show the internal force predictive model of three fingers. R-squared values of the polynomial regressions are 0.984, 0.976, 0.9947 for finger 1, finger 2, finger 3 respectively. The right figures show the error between the measured data and the predicted value. Based on the error, a threshold is set to detect the contact. The value of the thresholds are 2 N, 0.4 N, 0.6 N for finger 1, finger 2 and finger 3 respectively._

is defined differently for different fingers, as shown in Figure 5.9. The use of these thresholds for detecting the contact will be evaluated in Section 5.5.

5.4 Estimating the actual contact force

With the predicted internal force, the actual contact force was then estimated using the hypothesis mentioned in Section 3.3.1. To prove the hypothesis, the relationship between the actual contact force, the real measurement, and the predicted internal force must be studied. The steps of the experiment are visualized in Figure 5.10.

Figure ***5.10*** *The figure shows steps of the experiment conducted to prove the proposed method for estimating the contact force.*
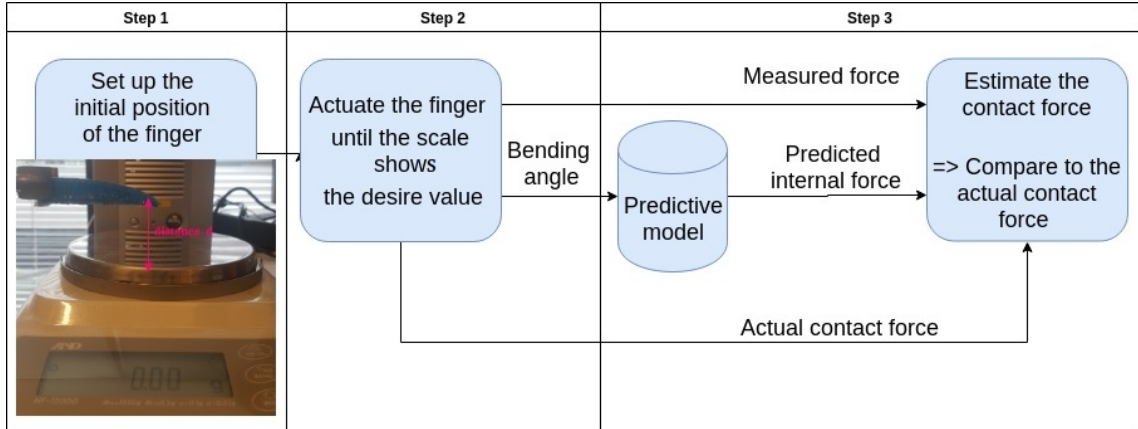
1. The finger with attached sensors was placed on top of a calibrated scale, with the distance "d" between the finger and the scale (initial position). At each distance, three cycles from step 2 to step 3 were conducted.

2. The finger was then actuated to press against the scale until the reading on the scale shows the desired value. The corresponded data that were bending angle and measured force, were saved at this moment.

3. The contact force was then estimated using Equation 3.13. After three cycles are done, the initial distance "d" between the finger and the scale was increased for the new cycle.

With the larger distance between the finger and the scale, the finger has to bend more towards the scale to make contact and cause the wanted force. That is the reason the last step was conducted as it studied how the force measurement behaved at different finger configurations.

In this experiment, two reference contact force values: 2 N and 4 N were considered. Figure 5.11 and Figure 5.12 show in both cases the relation between the real measurement, the internal force, and the estimated contact force. From the left plots, it is seen that regardless of the initial position of the finger, the difference

between the real measurement and the predicted internal force seems to remain the same in both cases. As stated earlier, this quantity is assumed to be the contact force. Thus, it is crucial to plot the quantity against the reference contact force for verifying the hypothesis. The plotted graphs on the right show that the estimate contact force, *i.e.*, the difference between the real measurement and the predicted force, slightly varies around the actual contact force. The error of this estimation, which ranges from 0.1 to 0.5 N at most, is within the tolerance for the objects we will later grasp, as explained in Chapter 5. Therefore, the proposed assumption of estimating the contact force by simply subtracting the internal force from the real measurement is shown to be sufficiently accurate.
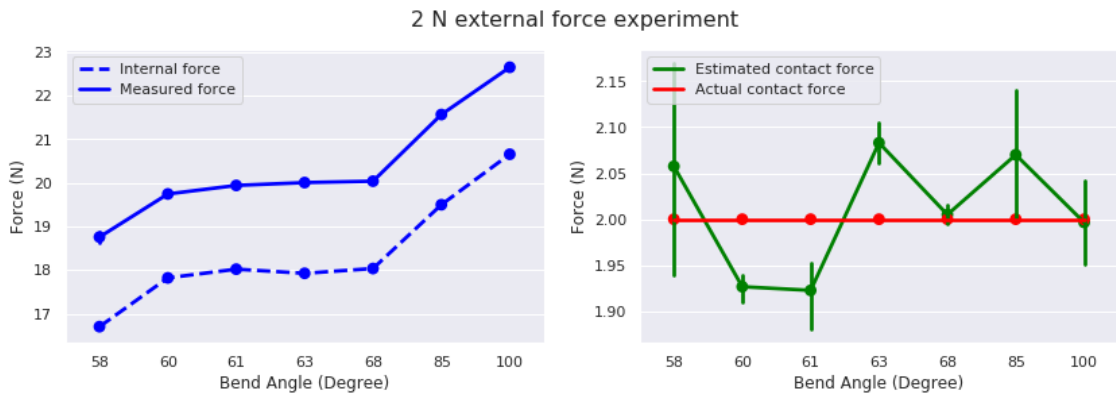

Figure 5.11 *The figure presents the result of the experiment in the 2 N case. The left figure shows the relation between the measured force and the predicted internal force. The right figure plots the estimated contact force against the actual contact force.*
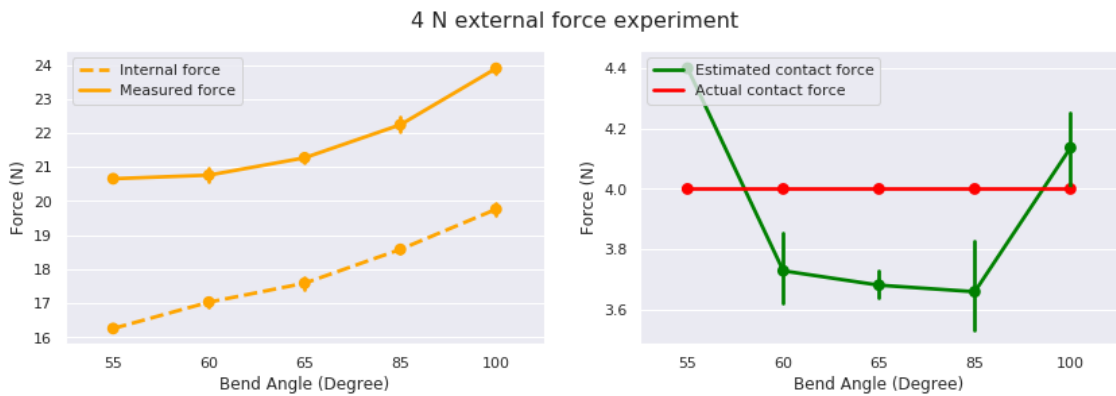

Figure 5.12 *The figure presents the result of the experiment in 4 N case.*

5.5 Contact detection using estimated contact force

The previous section concluded that a threshold needs to be defined to safely detect contact between a soft finger and an object. If the estimated contact force of the soft finger exceeds a defined threshold, there is a contact between the finger and the object. The contact detection using the estimated contact force and the defined threshold was examined through an experiment. In this experiment, finger 2 of the soft hand was first actuated in free space and then to be in contact with a solid object at 40% duty cycle. The threshold to safely detect the contact for finger 2 was set to 2 N, as shown in Figure 5.9. Figure 5.13 shows the estimated contact force in both cases, and the contact detected using the defined threshold. It is seen

Figure 5.13 *The figure shows the estimated contact force when the finger bends in free space (blue line) and when the finger makes contact with objects (orange line). The solid red line shows the moment when contact actually happens while the dashed red line shows the moment when the system detects the contact.*

from the figure that the estimated contact force in both cases varies around the value of zero when the finger does not make contact with any object. This means that the internal force predictor has successfully predicted the internal force with minor error. As the contact detection threshold for this finger is 2 N, the moment of contact is detected at 44 % duty cycle. Since the finger was inflated by incrementing the duty cycle by 2 % every 200 ms and the actual contact happens at 40 % duty cycle, a delay of around 400 ms was introduced. In other words, with the defined threshold, the system is able to detect the contact between the finger and the object 400 ms after it actually occurred. The result is good despite the small delay. It is indeed possible to set a lower threshold to detect the contact faster, but this is also considered risky as the error may exceed the threshold when the finger is not in contact with any objects. Thus, a trade-off between the delay and the accuracy

of contact detection is inevitable. Therefore, the threshold should be chosen in such a manner to accurately detect the contact with minimal delay.

5.6 Estimating object properties

The goal of this experiment is to study if the feedback of the embedded sensors can estimate the stiffness of an object. According to Yuan [70], the most important factor to estimate the hardness of an object is the relationship between the geometry of the deformed object and the pressing force. When pressing on harder objects, they deform less compared to soft objects, thus retaining larger slopes on the contact surface [70]. In this work, the estimated contact force is seen as the pressing force, and the bending angle of the finger is considered as the deformation of the object. This experiment investigates whether the relationship between the two can be used to realize the hardness of an object.

To this end, the finger was actuated to make contact with two objects with different hardness. A solid spray can, and a woolly hat shown in Figure 5.14 were selected as target objects. The target objects were placed in such a way that they

Figure 5.14 *The top figure shows the two target objects in this experiment: a woolly hat and a spray can. Bottom figures show the experimental setup for both objects.*

will be in contact with the finger at 40% duty cycle, as shown in Figure 5.14. The

sensory readings were then recorded. Figure 5.15 shows the estimated contact force against the duty cycle in both cases. From the figure, two different force profiles
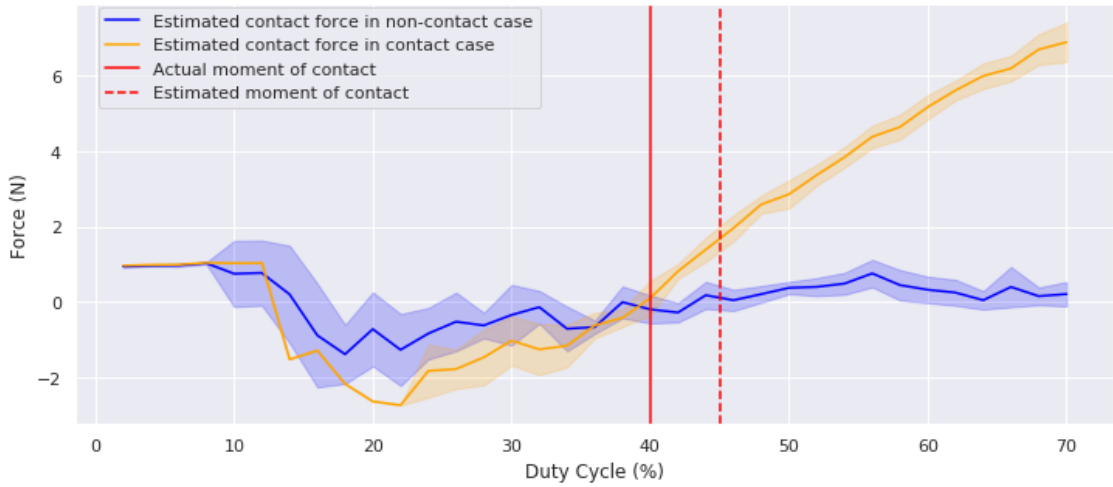

Figure 5.15 *The figure shows the estimated contact force when the finger bends in free space (blue line) and when the finger makes contact with the spray can (orange line) and the woolly hat (green line). The red line shows the moment when the contact actually happens while the red dashed line shows the moment when the system detects the contact.*

are clearly observed. The orange and green lines represent the estimated contact force of the finger when it makes contact with the spray can (solid object) and the woolly hat (soft object), respectively. The force profile of the spray can is steeper than that of the woolly hat. While the spray can constrain the bending of the finger after the contact, the woolly hat allows the finger to continue to bend towards the object. As the finger continues to bend after the contact with the woolly hat, the internal force increases, which leads to the reduction in the estimated contact force. Thus, the estimated contact force in the case of the woolly hat is smaller than that of the spray can. Therefore, the contact force profile of the solid object is steeper compared to that of the soft object.

To make it easier to distinguish between the solid object and the soft object from the sensory reading, the relationship between the bending angle and the contact force was studied. Figure 5.16 plots the bending angle against the estimated contact force in both cases. It is seen from the figure that in the case of the spray can the bend angle remains almost constant while the contact force continues to increase. This means that the finger has been stopped by something stiff. And since the finger is kept actuating, it keeps pressing stronger against that stiff object resulting in the increase of the contact force. However, in the case of the woolly hat, both the bending angle and the contact force increase simultaneously after the contact. This indicates that the target object is not stiff enough to constrain the bending of the
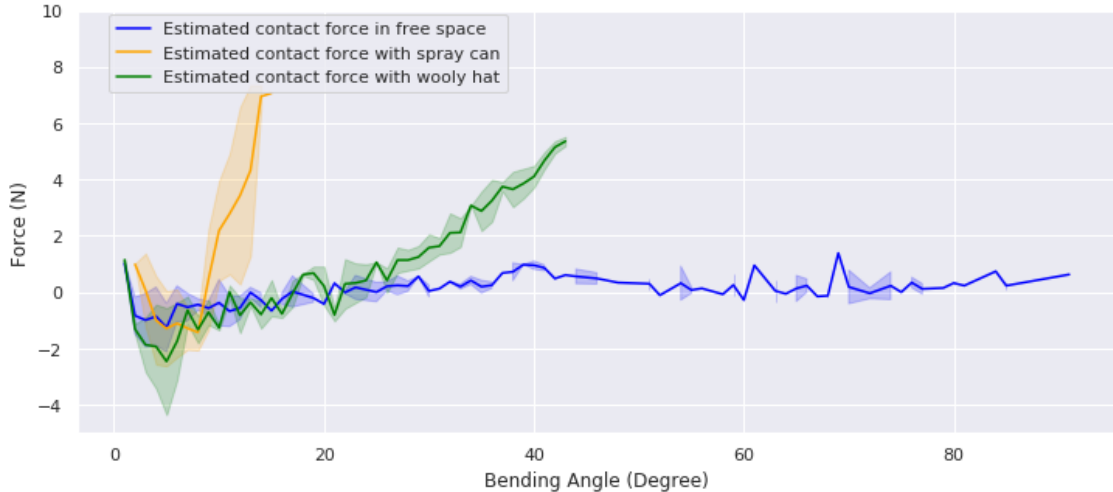
Figure 5.16 _The blue line represents the estimated contact force when the finger bends in free space. The orange and green line represent the estimated contact force when the finger makes contact with the spray can and the woolly hat, respectively._

finger after contact. Based on these results, it seems that the soft finger embedded with selected sensors can successfully distinguish between a solid object and a soft object using only the sensory feedback.

Given the fact that the sensory feedback provides valuable data to distinguish between a solid object and a soft object, can it be used to distinguish between a soft object and a very soft object? To answer this question, the same experiment was repeated but with an object stiffer than the woolly hat but softer than the spray can. The new target object selected was a plastic cup. Figure 5.17 plots the sensory reading obtained in the case of the plastic cup against that of the spray can and the woolly hat. From the figure, it is observed that the plastic cup can be clearly distinguished from the spray can using the sensor readings. However, the difference between the sensory feedback of the plastic cup and that of the woolly hat is minimal. In the case of the plastic cup, the bending angle of the finger can only reach to 30° while the woolly hat allows the finger to bend much further. This, to some extent, indicates that the woolly hat is softer than the plastic cup. However, as stated earlier in this section, the slope of the sensory reading is one of the most important clues to realize the hardness of an object. As seen in the figure, the slopes of the sensory reading in the case of the plastic cup and the woolly hat are not that different. This may provide an inaccurate result in distinguishing between a soft object and a very soft object.

In conclusion, the feedback of the selected sensors provides reliable data to distinguish between a solid object and a soft object. However, it is not safe to use this data for distinguishing between soft objects.
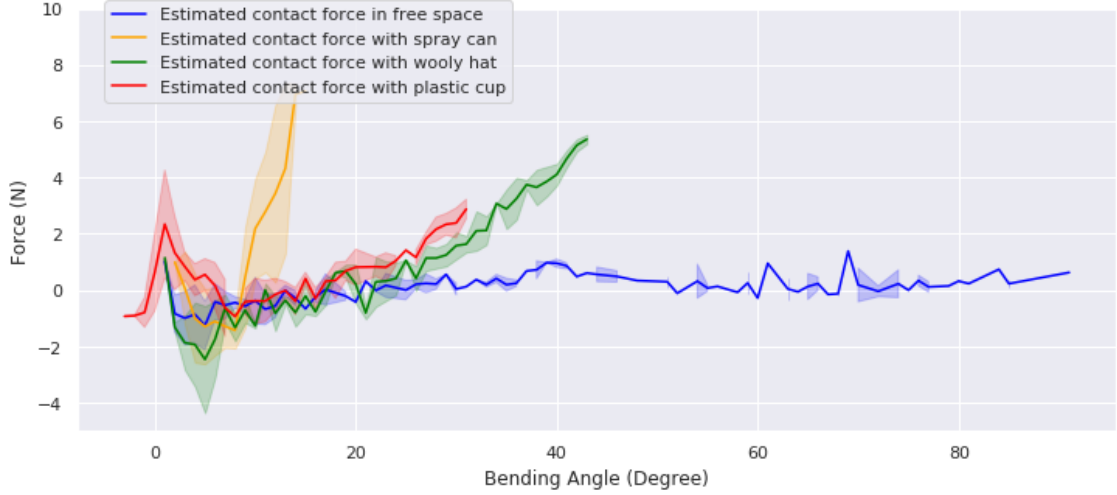
Figure ***5.17*** *The figure shows the sensory feedback of all target objects including the plastic cup (red line).*

5.7 Direct force controller

To control the soft hand to interact with objects at a specific contact force, a direct force controller mentioned in Section 3.4 was developed. To evaluate the accuracy and stability of the proposed controller, a series of experiments were conducted.

Influence of the controller gains

As the influence of the controller gains is crucial to the behaviour of the controller, an experiment was conducted to find the suitable value of the controller gains. In this experiment, the force controller was first experimented and evaluated with different values of the gains on one finger. The experiment used the same setup shown in Figure 5.14, in which the spray can was placed near the finger to ensure that contact between the two would happen. Two target contact forces: 2.5 N and 4 N were set in this experiment. Starting from 0% duty cycle, the finger was inflated by increasing the duty cycle by 2% every 200 ms until it made contact with the spray can. At that point, the force controller was activated, and it started to regulate the duty cycle to achieve the target contact force between the finger and the spray can. This was performed for two gain settings: $K_p = 20$, $K_i = 3$ and $K_p = 10$, $K_i = 1.5$.

Figure 5.18 shows two sets of gain and their influence on the system behaviour. It is noticeable that when the proportional and integral gains were set to $K_p = 20$ and $K_i = 3$ respectively, the measured contact force fluctuated abruptly. Nevertheless, the measured contact force remained stable when both of the gains were reduced to half. Specifically, in the case of 2.5 N target contact force, the root mean square

error (RMSE) was significantly reduced from 0.48 N to 0.13 N by changing the gain setting from $K_p = 20$, $K_i = 3$ to $K_p = 10$, $K_i = 1.5$. Similarly to the first case, in the case of 4 N target contact force, the RMSE was also reduced from 0.6 N to 0.3 N by making the same adjustment. Based on the experiment result, the controller gains were set to $K_p = 10$ and $K_i = 1.5$ to provide the best outcome for the next experiments.
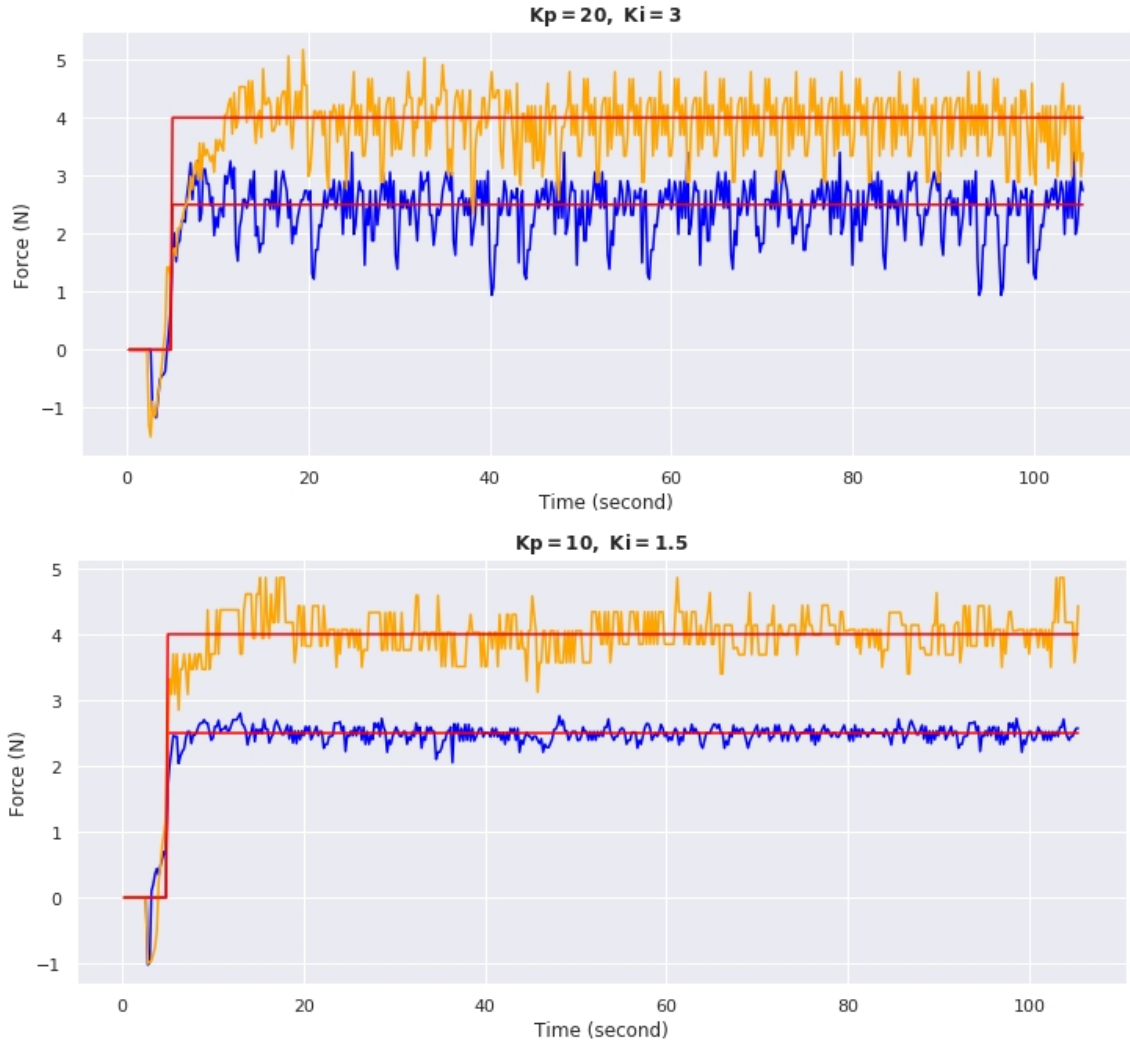
Figure 5.18 *The figure shows the controller behaviour with different sets of controller gains. Two target contact forces: 2.5 N, 4 N, were used in this experiment.*

The accuracy of the developed force controller

In order to test the accuracy and stability of the force controller in achieving the target contact force, the controller was first tested on only one finger of the soft hand The force controller scheme is shown in Figure 4.10. In this experiment, with 65 kPa pressure input, the finger was first actuated from 0% to make contact with the

spray can. The sensory feedback from the embedded flex sensors was continuously fed to the derived regression model to estimate the actual contact force. When contact with the spray can was detected, the force controller was activated. For this force controller, the proportional and integral gains were set to $K_p = 10$ and $K_i = 1.5$, respectively, which were the values that were experimentally found to provide the best outcome. The difference between the target and current contact force was then fed to the PI controller as the error signal. Based on this error, the PI controller calculated the corresponding amount to be added to (or subtracted from) the current duty cycle signal. The new duty cycle signal drove the finger to achieve the target contact force.

Figure 5.19 shows the contact force response and the duty cycle output from the controller when testing the finger at 65 kPa pressure input, and the target contact force is 2.5 N. The yellow region in the figure illustrates the duration when
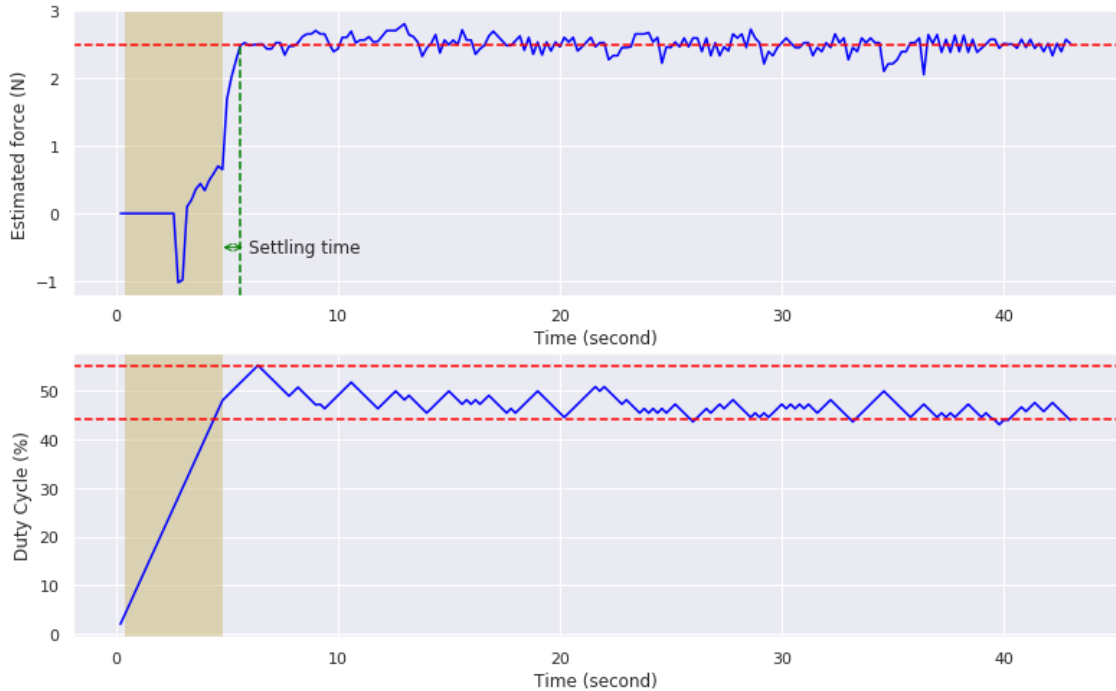
Figure 5.19 *The figure shows the contact force response against the change in the duty cycle of PWM signal. The top figure shows the contact force response of the force controller. In this figure, the red dashed line represents the target contact force: 2.5 N, and the green arrow indicates the setting time. The bottom figure shows the change in the duty cycle to achieve the target contact force.*

the force controller was activated. It can be observed from the top figure that the contact force response settled to a value approximately 2.5 N (red dashed line in the top figure) in roughly 800 milliseconds (ms) (green arrow in the top figure). This qualitative evaluation was supported by the RMSE of 0.21 N between the measured

and the target contact force. From the bottom figure, it is noticeable that the controller regulated the duty cycle value in the range of 45% - 55% (red dashed line in the bottom figure) to achieve the target contact force. The main reason for the fluctuations in the output duty cycle is the fluctuations in the estimated contact force response caused by the residual oscillations in the sensory reading. Regardless of the small fluctuations in the contact force and the output duty cycle, the developed force controller was successful in controlling the soft finger to achieve the target contact force in a reasonable settling time.

The proposed controller was further tested on all fingers of the soft hand simultaneously. In this experiment, the target contact force was fed to the force controller as a step reference signal. The step reference signal increased from 0 to 3 N and then fall back to 2 N. Three fingers were first actuated from 0% until one of the fingers detected the contact. At this point, the force controller was activated. Figure 5.20 shows the contact force response of all the fingers. It is noticeable that the contact force response of three fingers closely followed the step reference signals with a RMSE of 0.134 N, 0.359 N, and 0.194 N, respectively. Furthermore, the settling time of three fingers was 400 ms, 1 s, and 800 ms, respectively. The results of these experiments confirmed that the contact force between the soft hand and objects could be controlled in an accurate and fast manner to follow a variable reference signal based on only the sensory feedback. In addition, a key feature of this controller is that it relies only on the feedback from the sensors (bend sensor and force sensor) that are directly integrated into the hand. Thus, the proposed method and approach can be used to control any soft hands integrated with the same type of sensor.

5.8 Grasping deformable planar objects

The previous experiments were conducted to evaluate the characteristics of selected sensors and the behaviour of the proposed control strategy. The results of the experiments show that it is possible to control the contact force between a soft hand and objects using only the feedback from embedded sensors. However, the question of why do we need to integrate sensors to the soft hand to manipulate objects was not answered. To answer this question, a final experiment was conducted, and it examined if a soft hand can successfully grasp deformable planar objects such as empty plastic cup without crushing or dropping them using the selected sensors and the proposed control strategy. The key factor in this problem is the grasping force, too big a grasping force causes damage to the objects while too small a grasping force leads to a failed grasp attempt. Thus, to successfully grasp deformable planar objects, a suitable grasping force needs to be fed to the gripper. The final experiment was conducted to find the minimum grasping force for grasping deformable planar
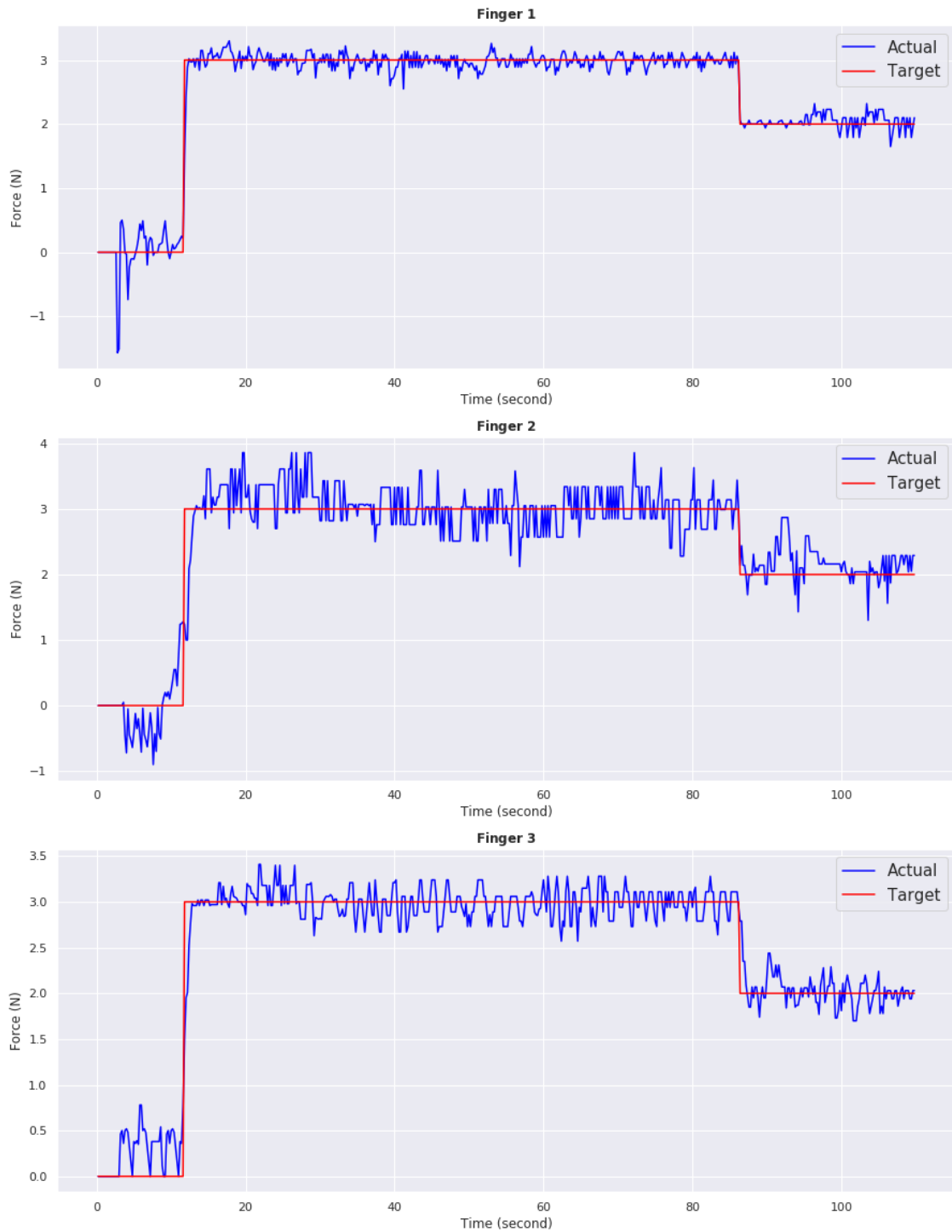
Figure 5.20 *Contact force response of three fingers to step reference signals.*

objects using the selected sensors and the proposed control strategy.

In this experiment, three objects shown in Figure 5.21, *i.e.*, an empty plastic cup, an empty paper cup and an empty eggshell, were used as target objects. The empty plastic cup and the empty paper cup represent deformable planar objects

Figure 5.21 *(a) The target objects in this experiment: an empty plastic cup, an empty paper cup, an empty eggshell (left to right). (b) The soft hand setup for this experiment.*

and the empty eggshell a fragile object. The setup of the soft hand was shown in Figure 5.21 b, in which the soft hand was fixed to a handle. The target contact force value was first set to a high value and then to smaller values. As stated earlier the soft hand contains three fingers where two fingers (Finger 1 and Finger 2 shown in Figure 4.1) are on one side and one finger (Finger 3) is on the opposite side. Thus, to stabilize the objects the targets contact forces of the three fingers were set in such a way that the sum of the contact force of Finger 1 and Finger 2 was equal to that of the Finger 3. In each case of the contact force, ten grasp attempts were made and the behaviour of the objects were observed and recorded. To evaluate if a grasp was successful, the soft hand first grasped the object until the target contact force was achieve, then we moved the handle upward 30 cm to lift the object, and then we rotated the hand $\pm 90^o$ around the x-axis (as shown in Figure 5.21 b). A grasp was considered to be successful when the grasped objects did not deform and slip away from the hand even under external disturbances.

The result of the final experiment is presented in Table 5.1 and Table 5.2. Table 5.1 shows the result in the case of the empty plastic cup and Table 5.2 shows that of

the empty paper cup. The green color columns in both tables indicate the minimum force to successfully grasp the target objects.

Target contact force (N)	2,2,4	1.5,1.5,3	1,1,2	0.75,0.75,1.5	0.5,0.5,1	0.25,0.25,0.5
Dropped Rate	0/10	0/10	0/10	0/10	0/10	6/10
Dropped Percentage	0%	0%	0%	0%	0%	60%
Deformed Rate	10/10	10/10	9/10	4/10	1/10	0/10
Deformed Percentage	100%	100%	90%	40%	10%	0%

Table 5.1 *The table shows the result in the case of the empty plastic cup. The green column shows the minimum contact forces of three fingers, i.e., 0.5 N, 0.5 N, 1 N, to successfully grasp the plastic cup without crushing (only 10% of deformed rate) and dropping the object (0% of dropped rate).*

Target contact force (N)	2,2,4	1.5,1.5,3	1,1,2	0.75,0.75,1.5	0.5,0.5,1	0.25,0.25,0.5
Dropped Rate	0/10	0/10	0/10	3/10	8/10	10/10
Dropped Percentage	0%	0%	0%	30%	80%	100%
Deformed Rate	10/10	8/10	2/10	1/10	0/10	0/10
Deformed Percentage	100%	80%	20%	10%	0%	0%

Table 5.2 *The table shows the result in the case of the empty paper cup. The green column shows the minimum contact forces of three fingers, i.e., 1 N,1 N,2 N, to successfully grasp the plastic cup without crushing (only 20% of deformed rate) and dropping the object (0% of dropped rate).*

It is observed from the tables that in both cases, the higher the contact force leads to lower dropped rate and higher deformed rate. However, to successfully grasp the object without crushing or dropping the objects, a contact force that provides the lowest dropped rate and the lowest deformed rate was selected. As the empty plastic cup is softer than the empty paper cup, the minimum force to successfully grasp the plastic cup should be smaller than that of the paper cup. This was proved by the result shown in the table, in which the minimum force in the case of the plastic cup is half of the one for the paper cup.

In addition, the experiment was also conducted on the eggshell to evaluate the proposed control strategy in the case of fragile objects. The result shows that the eggshell can not be damaged even with maximum contact forces. Thus, a soft hand

embedded with sensors is redundant in the case of fragile objects. However, earlier results shown in Table 5.1 and Table 5.2 show that the deformable planar objects can be crushed even with soft hands when high force is used. Specifically, when we applied 2 N, 2 N, and 4 N of force, respectively to three fingers of the soft hand, both the empty plastic cup and the empty paper cup were crushed. This emphasizes the need for integrating sensors to soft hands to manipulate deformable planar objects.

5.9   Discussion

All the experiments presented in this chapter aimed to evaluate the selected sensors and the proposed control strategy for the soft hand. The performance of the main functionalities was confirmed. The first experiment (Section 5.1) evaluated the characteristics of the selected sensors. The sensors were able to provide valuable and repeatable data, *i.e.*, the bending angle, and the applied force. In addition, the experiment pointed out the problem of the selected force sensor. The second experiment (Section 5.2) showed the effectiveness of the developed pneumatic LPF on smoothing the pressure signal and the sensory reading. The third experiment (Section 5.3) verified the predictor for predicting the internal force caused by bending. The internal force was extremely important in estimating the actual contact force between the hand and objects. The fourth experiment (Section 5.4) proved the proposed hypothesis for estimating the actual contact force. With the estimated contact force, the fifth experiment (Section 5.5) showed the use of the quantity in contact detection. The sixth experiment (Section 5.6) presented the possibility of realizing the hardness of objects using the selected sensors. The seventh experiment (Section 5.7) showed that it is possible to control the contact force in real-time. Last but not least, the final experiment demonstrated the need for integrating sensors into the soft hand to manipulate deformable planar objects. In addition to these experiments, several experiments were conducted to test different characteristics of the selected sensors. In one of these additional experiments, the slip detection was tested. The result showed that the slip could not be detected using this set of sensor as the force sensor was not sensitive to tangential force.

The reliability of the flex bend sensor was reported in [15]. This was further supported by the results of our experiments. The results showed that both selected sensors provided repeatable responses after a number of repetitions. This indicated the high reliability of the selected sensors. Furthermore, the results also showed that the sensors successfully provided accurate measurements compared to the ground truth value. Yet the force sensor performed well only in stationary situations. In particular, when the force sensor was bent, it introduced what we termed internal force, and this quantity was undesirable. To mitigate this issue, we introduced an

approach to compensate for the internal force, and to estimate the contact force. This approach was evaluated by an experiment and the result showed that the contact force was still sufficiently estimated. All in all, with the proposed approach, the force sensor was proved to give sufficient contact force even when it is bent.

The obtained results suggested that the interaction between the soft hand and objects or the environment can be studied by using only embedded sensors. In particular, the system is able to successfully grasp deformable planar objects without crushing or dropping them. As the sensors were directly integrated into the hand, the same approach can be applied to other soft robotic hands. However, more experiments are required to evaluate the performance of the proposed control strategy and selected sensors in more complex manipulation tasks such as in-hand manipulation.

6 Conclusions

The objectives of this thesis were to integrate appropriate sensors into a soft robotic hand and to develop a control strategy using only the sensory feedback for investigating the interaction between the soft hand and objects. Achieving these goals is a step towards showing that soft hands are able to not only grasp in the same manner as humans but also perform useful actions with grasped objects.

This thesis was split into a theoretical part presented in Chapter 2, a research methodology part in Chapter 3 and a more practical part presenting the testbed and experimental evaluation.

From the background theory, we observed that the majority of the works on soft robotic hands focus on the hand design rather than the control aspect. Soft hands were usually claimed to successfully grasp a wide range of objects. However, the target objects were typically rigid. This raised a question of whether we can manipulate deformable objects with soft hands. To accomplish this task, the interaction between the hand and objects (or contact force) is vital as deformable objects can be easily crushed even with soft hands when high contact force is used. Therefore, this work attempted to tackle this problem by integrating sensing capability into the soft hand to study the interaction between the soft hand and objects. In this work, we focus on selecting suitable sensors, then characterizing them to extract the desired information, in this case, contact force, and studying how to control the contact force to achieve complex manipulation tasks.

The research methodology part started by presenting the characterization process of the chosen sensors: resistive flex bend and force sensor. While the bend sensor provided reliable data, the force sensor introduced a problem of producing internal force measurement when it is bent. To combat this issue, we proposed the method discussed in Chapter 3 to estimate the actual contact force from the sensory feedback. The contact force estimating and the design of the proposed control strategy represent the core of this work. The sensing of contact force allows the detection of contact between the soft hand with objects or the environment. The control strategy used the switching control mechanism to choose the appropriate controller for each phase of the grasping, improving the quality of the grasp. Specifically, the force controller was activated only when the contact between the hand and objects was detected.

The performance of the proposed approach was tested in the experiments using the developed soft hand and controller board. The results were satisfactory. The proposed approach was able to control the contact force in real-time, using only sensory feedback from selected sensors. Nevertheless, the implemented system in

this work also had its limitations. For the sensors, while the bend sensor provided valuable readings, the force sensor introduced a problem when it is bent. In addition, more complex manipulation tasks such as in-hand manipulation required the force measurements at different sections of the finger while the selected force sensor gave only one measurement along the body of the finger. Another limitation of the system was the object deformation tracking as at the moment the deformation of objects was observed manually by the human. With all of this in mind, future extensions to improve the system built in this thesis should concentrate on:

- considering the feedback from the internal pressure sensor as another input for estimating the actual contact force. This helps to provide a more robust system that can handle external disturbances in terms of pressure leaks.

- adding the object deformation detection by visual information from a high rate camera.

- learning the minimum grasping force for deformable planar objects. In this work, the minimal grasping force for each object was found manually by experimenting with different values. With the development of the suggested object deformation detection, the minimal grasping force of different objects can be learned.

Other possibilities for a soft robotic hand with embedded sensors, which may be different from the one used in this thesis, are to:

- estimate the properties of the grasped objects. As the experiment conducted in Section 5.6 proved the possibility of estimating the stiffness of an object, this can be further studied and expanded to other properties of the grasped objects such as size, shape, position, and orientation.

- learn to achieve more complex manipulation tasks such as in-hand manipulation.

The research on achieving complex manipulation tasks such as in-hand manipulation using soft robotic hands are still limited. To achieve those tasks, sensory feedback and reinforcement learning are usually used. However, the lack of sensing capabilities and simulation model of soft robotic hands have constrained the research on this matter. This work proved that it is possible to study the interaction between the soft hand and objects using only simple and commercial sensors. Hopefully, with the development of simulation models of soft robotic hands and the sensors, the research on complex manipulation skills with soft robotic hands will progress further.

All in all, this thesis showed that the interaction between a soft robotic hand and objects or the environment in terms of contact force could be studied by integrating inexpensive commercial sensors to the hand. In addition, the thesis proved that the contact force could be successfully controlled in real-time to interact with objects. This work, together with the proposed future works, will contribute towards expanding the application of soft robotic hands, including more sophisticated manipulation tasks. This, together with the safety inherited from the softness properties of the hand might leads to more service robots in human environments.

References

[1] Sreejan Alapati and Shivraj Yeole. "A Review on Applications of Flex Sensors". In: *International Journal of Emerging Technology and Advanced Engineering* 7 (July 2017), pp. 97–100.

[2] *Bayesian information criterion.* https://en.wikipedia.org/wiki/Bayesian_information_criterion. Accessed: 2019-08-2.

[3] R. Adam Bilodeau, Edward L. White, and Rebecca K. Kramer. "Monolithic fabrication of sensors and actuators in a soft robotic gripper". In: *2015 IEEE/RSJ International Conference on Intelligent Robots and Systems (IROS)* (2015), pp. 2324–2329.

[4] Phil Britt. *Food Industry Use of Robotics to Grow Sharply.* Jan. 2018. URL: https://www.roboticsbusinessreview.com/manufacturing/food-industry-use-robotics-grow-sharply/.

[5] C. Choi et al. "Learning Object Grasping for Soft Robot Hands". In: *IEEE Robotics and Automation Letters* 3.3 (July 2018), pp. 2370–2377. ISSN: 2377-3766. DOI: 10.1109/LRA.2018.2810544.

[6] R. Deimel and O. Brock. "A compliant hand based on a novel pneumatic actuator". In: *2013 IEEE International Conference on Robotics and Automation.* May 2013, pp. 2047–2053. DOI: 10.1109/ICRA.2013.6630851.

[7] Raphael Deimel. "Soft robotic hands for compliant grasping". Doctoral dissertation. 2017. URL: http://dx.doi.org/10.14279/depositonce-6063.

[8] Raphael Deimel and Oliver Brock. "A Novel Type of Compliant and Underactuated Robotic Hand for Dexterous Grasping". In: *Int. J. Rob. Res.* 35.1-3 (Jan. 2016), pp. 161–185. ISSN: 0278-3649. DOI: 10.1177/0278364915592961.

[9] Raphael Deimel and Oliver Brock. *RBO Hand 2 CAD Files.* 2017. DOI: 10.14279/depositonce-5831.

[10] Ángel Delgado et al. "Control of Robot Fingers with Adaptable Tactile Servoing to Manipulate Deformable Objects". In: *Robot 2015: Second Iberian Robotics Conference.* Ed. by Luís Paulo Reis et al. Cham: Springer International Publishing, 2016, pp. 81–92. ISBN: 978-3-319-27146-0.

[11] A. Delgado et al. "A tactile-based grasping strategy for deformable objects' manipulation and deformability estimation". In: *2015 12th International Conference on Informatics in Control, Automation and Robotics (ICINCO).* Vol. 02. July 2015, pp. 369–374.

[12] Tom Dietterich. "Overfitting and Undercomputing in Machine Learning". In: *ACM Comput. Surv.* 27.3 (Sept. 1995), pp. 326–327. ISSN: 0360-0300. DOI: 10. 1145/212094.212114. URL: http://doi.acm.org/10.1145/212094.212114.

[13] Aaron M. Dollar and Robert D. Howe. "The Highly Adaptive SDM Hand: Design and Performance Evaluation". In: *The International Journal of Robotics Research* 29.5 (2010), pp. 585–597. DOI: 10.1177/0278364909360852.

[14] *EGaIn Sensors*. https://softroboticstoolkit.com/book/egain-sensors. Accessed: 2019-02-18.

[15] Khaled Elgeneidy, Niels Lohse, and Michael Jackson. "Bending angle prediction and control of soft pneumatic actuators with embedded flex sensors - A data-driven approach". In: *Mechatronics* 50 (2018), pp. 234–247. ISSN: 0957-4158. DOI: https://doi.org/10.1016/j.mechatronics.2017.10.005.

[16] George Ellis. "Chapter 10 - Introduction to Observers in Control Systems". In: *Control System Design Guide (Fourth Edition)*. Ed. by George Ellis. Fourth Edition. Boston: Butterworth-Heinemann, 2012, pp. 185–212. ISBN: 978-0-12-385920-4. DOI: https://doi.org/10.1016/B978-0-12-385920-4.00010-2. URL: http://www.sciencedirect.com/science/article/pii/B9780123859204000102.

[17] *Fiber-Reinforced Actuators*. https://softroboticstoolkit.com/book/fiber-reinforced-bending-actuators. Accessed: 2019-06-25.

[18] *Flex Sensor Hookup Guide*. https://learn.sparkfun.com/tutorials/flex-sensor-hookup-guide/. Accessed: 2019-03-25.

[19] "Force Control". In: *Robotics: Modelling, Planning and Control*. London: Springer London, 2009, pp. 363–405. ISBN: 978-1-84628-642-1. DOI: 10.1007/978-1-84628-642-1_9. URL: https://doi.org/10.1007/978-1-84628-642-1_9.

[20] *Force Sensitive Resistor Hookup Guide*. https://learn.sparkfun.com/tutorials/force-sensitive-resistor-hookup-guide?_ga=2.237839236.560186083.1560968106-1498892360.1546944131. Accessed: 2019-03-25.

[21] G. L. Foresti and F. A. Pellegrino. "Automatic visual recognition of deformable objects for grasping and manipulation". In: *IEEE Transactions on Systems, Man, and Cybernetics, Part C (Applications and Reviews)* 34.3 (Aug. 2004), pp. 325–333. ISSN: 1094-6977. DOI: 10.1109/TSMCC.2003.819701.

[22] Barbara Frank et al. "Learning Deformable Object Models for Mobile Robot Path Planning using Depth Cameras and a Manipulation Robot". In: (Dec. 2010).

[23] A. Gupta et al. "Learning dexterous manipulation for a soft robotic hand from human demonstrations". In: *2016 IEEE/RSJ International Conference on Intelligent Robots and Systems (IROS)*. Oct. 2016, pp. 3786–3793. DOI: `10.1109/IROS.2016.7759557`.

[24] S. Hirai, T. Tsuboi, and T. Wada. "Robust grasping manipulation of deformable objects". In: *Proceedings of the 2001 IEEE International Symposium on Assembly and Task Planning (ISATP2001). Assembly and Disassembly in the Twenty-first Century. (Cat. No.01TH8560)*. May 2001, pp. 411–416. DOI: `10.1109/ISATP.2001.929069`.

[25] Richard Hodson. "How robots are grasping the art of gripping". In: *Nature* 557 (May 2018), S23–S25. DOI: `10.1038/d41586-018-05093-1`.

[26] B. S. Homberg et al. "Haptic identification of objects using a modular soft robotic gripper". In: *2015 IEEE/RSJ International Conference on Intelligent Robots and Systems (IROS)*. Sept. 2015, pp. 1698–1705. DOI: `10.1109/IROS.2015.7353596`.

[27] Bianca S. Homberg et al. "Robust Proprioceptive Grasping with a Soft Robot Hand". In: *Auton. Robots* 43.3 (Mar. 2019), pp. 681–696. ISSN: 0929-5593. DOI: `10.1007/s10514-018-9754-1`. URL: `https://doi.org/10.1007/s10514-018-9754-1`.

[28] A. M. Howard and G. A. Bekey. "Intelligent learning for deformable object manipulation". In: *Proceedings 1999 IEEE International Symposium on Computational Intelligence in Robotics and Automation. CIRA'99 (Cat. No.99EX375)*. Nov. 1999, pp. 15–20. DOI: `10.1109/CIRA.1999.809935`.

[29] Filip Ilievski et al. "Soft Robotics for Chemists". In: *Angewandte Chemie International Edition* 50.8 (2011), pp. 1890–1895. DOI: `10.1002/anie.201006464`.

[30] Mirna Issa et al. "Sensor elements made of conductive silicone rubber for passively compliant gripper". In: *International Journal of Advanced Manufacturing Technology* 69 (July 2013). DOI: `10.1007/s00170-013-5085-8`.

[31] Alexander Jung. "Machine Learning: Basic Principles". In: *arXiv e-prints*, arXiv:1805.05052 (May 2018), arXiv:1805.05052. arXiv: `1805.05052 [cs.LG]`.

[32] M. Kaboli, K. Yao, and G. Cheng. "Tactile-based manipulation of deformable objects with dynamic center of mass". In: *2016 IEEE-RAS 16th International Conference on Humanoid Robots (Humanoids)*. Nov. 2016, pp. 752–757. DOI: `10.1109/HUMANOIDS.2016.7803358`.

[33] F. F. Khalil and P. Payeur. "Robotic Interaction with Deformable Objects under Vision and Tactile Guidance - a Review". In: *2007 International Workshop on Robotic and Sensors Environments*. Oct. 2007, pp. 1–6. DOI: 10.1109/ROSE.2007.4373965.

[34] J. M. Krahn, F. Fabbro, and C. Menon. "A Soft-Touch Gripper for Grasping Delicate Objects". In: *IEEE/ASME Transactions on Mechatronics* 22.3 (June 2017), pp. 1276–1286. ISSN: 1083-4435. DOI: 10.1109/TMECH.2017.2663322.

[35] Jochen Lang, Dinesh K. Pai, and Robert J. Woodham. "Acquisition of Elastic Models for Interactive Simulation". In: *The International Journal of Robotics Research* 21.8 (2002), pp. 713–733. DOI: 10.1177/027836402761412458. eprint: https://doi.org/10.1177/027836402761412458. URL: https://doi.org/10.1177/027836402761412458.

[36] Z. Lazher et al. "Modeling and analysis of 3D deformable object grasping". In: *2014 23rd International Conference on Robotics in Alpe-Adria-Danube Region (RAAD)*. Sept. 2014, pp. 1–8. DOI: 10.1109/RAAD.2014.7002259.

[37] C Majidi, R Kramer, and R J Wood. "A non-differential elastomer curvature sensor for softer-than-skin electronics". In: *Smart Materials and Structures* 20.10 (Aug. 2011), p. 105017. DOI: 10.1088/0964-1726/20/10/105017.

[38] A. D. Marchese et al. "Design and control of a soft and continuously deformable 2D robotic manipulation system". In: *2014 IEEE International Conference on Robotics and Automation (ICRA)*. May 2014, pp. 2189–2196. DOI: 10.1109/ICRA.2014.6907161.

[39] Andrew D. Marchese, Cagdas D. Onal, and Daniela Rus. "Autonomous Soft Robotic Fish Capable of Escape Maneuvers Using Fluidic Elastomer Actuators". In: *Soft Robotics* 1.1 (2014). PMID: 27625912, pp. 75–87. DOI: 10.1089/soro.2013.0009. URL: https://doi.org/10.1089/soro.2013.0009.

[40] R. Maruyama, T. Watanabe, and M. Uchida. "Delicate grasping by robotic gripper with incompressible fluid-based deformable fingertips". In: *2013 IEEE/RSJ International Conference on Intelligent Robots and Systems*. Nov. 2013, pp. 5469–5474. DOI: 10.1109/IROS.2013.6697148.

[41] M. Memarian, R. Gorbet, and D. Kulic. "Control of soft pneumatic finger-like actuators for affective motion generation". In: *2015 IEEE/RSJ International Conference on Intelligent Robots and Systems (IROS)*. Sept. 2015, pp. 1691–1697. DOI: 10.1109/IROS.2015.7353595.

[42] Yiğit Mengüç et al. "Wearable Soft Sensing Suit for Human Gait Measurement". In: *Int. J. Rob. Res.* 33.14 (Dec. 2014), pp. 1748–1764. ISSN: 0278-3649. DOI: `10.1177/0278364914543793`. URL: `http://dx.doi.org/10.1177/0278364914543793`.

[43] J. Morrow et al. "Improving Soft Pneumatic Actuator fingers through integration of soft sensors, position and force control, and rigid fingernails". In: *2016 IEEE International Conference on Robotics and Automation (ICRA)*. May 2016, pp. 5024–5031. DOI: `10.1109/ICRA.2016.7487707`.

[44] Toshihiro Nishimura et al. "Fluid Pressure Monitoring-Based Strategy for Delicate Grasping of Fragile Objects by A Robotic Hand with Fluid Fingertips". In: *Sensors* 19 (Feb. 2019), p. 782. DOI: `10.3390/s19040782`.

[45] Y. Park, B. Chen, and R. J. Wood. "Design and Fabrication of Soft Artificial Skin Using Embedded Microchannels and Liquid Conductors". In: *IEEE Sensors Journal* 12.8 (Aug. 2012), pp. 2711–2718. ISSN: 1530-437X. DOI: `10.1109/JSEN.2012.2200790`.

[46] Yong-Lae Park et al. "Hyperelastic pressure sensing with a liquid-embedded elastomer". In: *Journal of Micromechanics and Microengineering* 20.12 (Nov. 2010), p. 125029. DOI: `10.1088/0960-1317/20/12/125029`. URL: `https://doi.org/10.1088/0960-1317/20/12/125029`.

[47] Dalibor Petković et al. "Adaptive Neuro Fuzzy Controller for Adaptive Compliant Robotic Gripper". In: *Expert Syst. Appl.* 39.18 (Dec. 2012), pp. 13295–13304. ISSN: 0957-4174. DOI: `10.1016/j.eswa.2012.05.072`.

[48] *PID controller*. `https://en.wikipedia.org/wiki/PID_controller`. Accessed: 2019-07-25.

[49] *Power Glove*. June 2019. URL: `https://en.wikipedia.org/wiki/Power_Glove#cite_note-8`.

[50] *Pulse-width modulation*. July 2019. URL: `https://en.wikipedia.org/wiki/Pulse-width_modulation`.

[51] Morgan Quigley, Brian Gerkey, and William D. Smart. *Programming Robots with ROS: A Practical Introduction to the Robot Operating System*. 1st. O'Reilly Media, Inc., 2015. ISBN: 1449323898, 9781449323899.

[52] Daniela Rus and Michael Tolley. "Design, fabrication and control of soft robots". In: *Nature* 521 (May 2015), pp. 467–75. DOI: `10.1038/nature14543`.

[53] Giovanni Saggio et al. "Resistive flex sensors: a survey". In: *Smart Materials and Structures* 25.1 (Dec. 2015), p. 013001. DOI: `10.1088/0964-1726/25/1/013001`. URL: `https://doi.org/10.1088/0964-1726/25/1/013001`.

[54] Jose Sanchez et al. "Robotic manipulation and sensing of deformable objects in domestic and industrial applications: a survey". In: *The International Journal of Robotics Research* 37.7 (2018), pp. 688–716. DOI: `10.1177/0278364918779698`. eprint: `https://doi.org/10.1177/0278364918779698`. URL: `https://doi.org/10.1177/0278364918779698`.

[55] S. Schulz, C. Pylatiuk, and G. Bretthauer. "A new ultralight anthropomorphic hand". In: *Proceedings 2001 ICRA. IEEE International Conference on Robotics and Automation (Cat. No.01CH37164)*. Vol. 3. May 2001, 2437–2441 vol.3. DOI: `10.1109/ROBOT.2001.932988`.

[56] Gideon Schwarz. "Estimating the Dimension of a Model". In: *The Annals of Statistics* 6.2 (1978), pp. 461–464. ISSN: 00905364. URL: `http://www.jstor.org/stable/2958889`.

[57] Jun Shintake et al. "Soft Robotic Grippers". In: *Advanced Materials* 30.29 (2018), p. 1707035. DOI: `10.1002/adma.201707035`. URL: `https://onlinelibrary.wiley.com/doi/abs/10.1002/adma.201707035`.

[58] Jun Shintake et al. "Versatile Soft Grippers with Intrinsic Electroadhesion Based on Multifunctional Polymer Actuators". In: *Advanced materials (Deerfield Beach, Fla.)* 28 (Nov. 2015). DOI: `10.1002/adma.201504264`.

[59] Deepak Trivedi et al. "Soft Robotics: Biological Inspiration, State of the Art, and Future Research". In: *Applied Bionics and Biomechanics* 5 (Oct. 2008), pp. 99–117. DOI: `10.1080/11762320802557865`.

[60] Zion Tse et al. "Soft Robotics in Medical Applications". In: *Journal of Medical Robotics Research* 03 (May 2018). DOI: `10.1142/S2424905X18410064`.

[61] Manuel R. Vegas and Jose L. Martin del Yerro. "Stiffness, Compliance, Resilience, and Creep Deformation: Understanding Implant-Soft Tissue Dynamics in the Augmented Breast: Fundamentals Based on Materials Science". In: *Aesthetic Plastic Surgery* 37.5 (Oct. 2013), pp. 922–930. ISSN: 1432-5241. DOI: `10.1007/s00266-013-0197-y`. URL: `https://doi.org/10.1007/s00266-013-0197-y`.

[62] D. M. Vogt, Y. Park, and R. J. Wood. "Design and Characterization of a Soft Multi-Axis Force Sensor Using Embedded Microfluidic Channels". In: *IEEE Sensors Journal* 13.10 (Oct. 2013), pp. 4056–4064. ISSN: 1530-437X. DOI: `10.1109/JSEN.2013.2272320`.

[63] *Voltage divider*. `https://en.wikipedia.org/wiki/Voltage_divider`. Accessed: 2019-07-25.

[64] V. Wall, G. Zoller, and O. Brock. "A method for sensorizing soft actuators and its application to the RBO hand 2". In: *2017 IEEE International Conference on Robotics and Automation (ICRA)*. May 2017, pp. 4965–4970. DOI: `10 . 1109/ICRA.2017.7989577`.

[65] Ernst Wit, Edwin van den Heuvel, and Jan-Willem Romeijn. "'All models are wrong...': an introduction to model uncertainty". In: *Statistica Neerlandica* 66.3 (2012), pp. 217–236. DOI: `10 . 1111 / j . 1467 - 9574 . 2012 . 00530 . x`. eprint: `https://onlinelibrary.wiley.com/doi/pdf/10.1111/j.1467-9574.2012.00530.x`. URL: `https://onlinelibrary.wiley.com/doi/abs/10.1111/j.1467-9574.2012.00530.x`.

[66] A. Yamaguchi and C. G. Atkeson. "Combining finger vision and optical tactile sensing: Reducing and handling errors while cutting vegetables". In: *2016 IEEE-RAS 16th International Conference on Humanoid Robots (Humanoids)*. Nov. 2016, pp. 1045–1051. DOI: `10.1109/HUMANOIDS.2016.7803400`.

[67] Akihiko Yamaguchi. "Assistive Utilities with FingerVision for Learning Manipulation of Fragile Objects". In: *19th SICE System Integration Division Annual Conference (SI2018)*. 2018.

[68] Akihiko Yamaguchi. *FingerVision*. `http://akihikoy.net/p/fv.html`. 2017.

[69] Akihiko Yamaguchi and Christopher G. Atkeson. "Grasp Adaptation Control with Finger Vision: Verification with Deformable and Fragile Objects". In: *35th Annual Conference of the Robotics Society of Japan (RSJ2017)*. Sept. 2017.

[70] W. Yuan, M. A. Srinivasan, and E. H. Adelson. "Estimating object hardness with a GelSight touch sensor". In: *2016 IEEE/RSJ International Conference on Intelligent Robots and Systems (IROS)*. Oct. 2016, pp. 208–215. DOI: `10 . 1109/IROS.2016.7759057`.